USING INFRASOUND TO CHARACTERIZE VOLCANIC EMISSIONS AT TOLBACHIK, KARYMSKY, AND SAKURAJIMA VOLCANOES

By

Sarah Albert

RECOMMENDED:

Dr. Curt Szuberla

Dr. Carl Tape

Dr. David Fee, Advisory Committee Chair

Dr. Paul McCarthy
Chair, Department of Geosciences

APPROVED:

Dr. Paul W. Layer
Dean, College of Natural Science and Mathematics

Dr. John C. Eichelberger
Dean of the Graduate School

27 July 2015
Date

USING INFRASOUND TO CHARACTERIZE VOLCANIC EMISSIONS AT TOLBACHIK, KARYMSKY, AND SAKURAJIMA VOLCANOES

A

THESIS

Presented to the Faculty

of the University of Alaska Fairbanks

in Partial Fulfillment of the Requirements

for the Degree of

MASTER OF SCIENCE

By

Sarah Albert, B.S.

Fairbanks, Alaska

August 2015

Abstract

The work presented herein includes one main body of research on infrasound from Tolbachik Volcano and suggestions for future work on eruption dynamics using infrasound from other volcanoes. We use both regional and local infrasound data to track the dynamics of the 2012-2013 eruption of Tolbachik Volcano, Kamchatka, Russia. Analysis of regional data recorded at the IMS array IS44 in southern Kamchatka, ~384 km from the vent, focuses on the eruption onset in November 2012, while analysis of local data recorded 100-950 m from the vent focuses on activity in February and August 2013. Signals recorded from Tolbachik suggest an increase in eruptive intensity occurred from November 28-29, 2012. Local infrasound data are characterized primarily by repeated, transient explosion signals indicative of gas slug bursts. Three methods are employed to pick slug burst events in February and August, with all methods proving to be effective. The nature of slug bursts makes a monopole acoustic source model particularly fitting, permitting volume outflux and slug radius calculations for individual events. Volume outfluxes and slug radii distributions provide three possible explanations for the eruption style of Tolbachik Volcano from mid-February to late August. Cumulative outflux for slug bursts (i.e. mass of emissions from individual bursts) derived by infrasound for both February and August range from <100 to 3000 kg. These values are greater than infrasound-derived emissions calculated at Pacaya Volcano, but less than those calculated at Mt. Erebus Volcano. From this, we determine slug bursts at Tolbachik Volcano in February and August were larger on average than those at Pacaya Volcano in 2010, but smaller on average than those at Mt. Erebus in 2008.

Suggestions for future work are also given after analysis of acoustic waveforms from local infrasound data collected at Karymsky and Sakurajima Volcanoes. Activity at both of these volcanoes ranges from short-duration ash-rich explosions to longer-duration ash-rich explosions. A multiparameter dataset collected at Karymsky Volcano in August 2011 includes infrasound data, gas and ash data, and thermal imagery from eruptive events. Content of gas vs. ash, general plume characteristics, plume altitude above the vent, plume temperature, and SO_2 emission rates are correlated with acoustic waveform families identified at each volcano using a cross correlation method. This preliminary analysis shows promise for correlating acoustic waveforms with eruptive activity and can likely be improved with future work.

Table of Contents

Page

List of Figures

List of Tables

Acknowledgments

I, Sarah Albert, am the sole author and have completed the research described in this thesis. Chapter 1 is a result of efforts from myself and the following co-authors:

David Fee[1], Pavel Firstov[2], Evgeniy Makhmudov[2], Pavel Izbekov[1]

who provided constructive criticism, helpful suggestions, and insightful discussion. From here on, all authors (including myself) will collectively be referred to as "we". For the sake of consistency, "we" is used throughout although no manuscript or coauthors are connected to future work. Fieldwork and assistance for this research was provided by the Institute of Volcanology and Seismology (IVS) and the Kamchatka Branch Geophysical Surveys (KGBS). It is with sincerest thanks that we acknowledge our colleagues at the University of Alaska Fairbanks (UAF), KBGS and IVS. Their efforts were extremely helpful in data collection and interpretation. We also thank those who participated in the collection of infrasound data from Sakurajima Volcano during the 2013 International Association of Volcanology and Chemistry of the Earths Interior (IAVCEI) post-conference volcano acoustics workshop.

Funding for this research was provided by the UAF Geophysical Institute, NSF EAR 1113338 (for research on Tolbachik Volcano), and NSF EAR 1331084 (for research on Karymsky and Sakurajima volcanoes). It is with sincerest thanks that we acknowledge our colleagues in the Seismology lab, the Alaska Volcano Observatory, and the Geology and Geophysics Department at the University of Alaska Fairbanks (UAF) for their constructive criticism and helpful comments.

First, thank you to my graduate advisor, Dr. Fee, for all of your help. Your encouragement and feedback allowed my education and research to flourish. Thanks to friends and colleagues for the memorable conversations and good times. To Kathleen McKee, my closest colleague, thank you for your friendship and support. Thank you Paul for putting up with my graduate student breakdowns and for encouraging me to get out of the office. And thank you Mom, Dad, Katie, and George for listening to my thoughts and for giving me motivation when I needed it most.

[1]Wilson Infrasound Observatories, Alaska Volcano Observatory, Geophysical Institute, University of Alaska Fairbanks, Fairbanks, AK USA

[2]Kamchatka Branch Geophysical Surveys, Petropavlovsk-Kamchatsky, Kamchatka, Russia

Introduction

I.1 Importance of Volcanic Emissions

Volcanic ash, gas, and tephra (rock fragments), referred to collectively as volcanic emissions, pose hazards to humans, livestock, and vegetation, are able to alter the climate as a whole, and can cause devastating effects to aircraft. The eruption of Mt. St. Helens in 1980 provided context for the destructiveness of volcanic ashfall on humans and sparked increased interest in the subject. Volcanic ash particles suspended in air have the ability to affect water quality, to affect soil toxicity for grazing animals, and to create physical and mental health challenges for humans (Cronin et al., 2000; Fraunfelder et al., 1983; Horwell and Baxter, 2006; Shore et al., 1986). Volcanic emissions can also contribute to a decrease in solar heating, essentially causing a global cooling effect (Soden et al., 2002).

Volcanic emissions pose a threat to jet aircraft, a pressing issue due to the amount of air traffic routes near potential volcanic ash paths. Ash from the 1989-1990 eruption of Redoubt Volcano, Alaska was intercepted by both commercial and military jet aircraft resulting in damages estimated to cost about $80 million (Casadevall, 1994). Similarly destructive encounters between jet aircraft and volcanic ash also occurred during the 1991 eruption of Mt. Pinatubo, Philippines, damaging 10 jet engines (Casadevall et al., 1996). In both the Redoubt and Mt. Pinatubo eruptions, serious damage and engine failure was a severe threat to passengers on commercial aircraft (Casadevall, 1994; Casadevall et al., 1996). The April 2010 eruption of Ejyafjallajokull Volcano in Iceland grounded and altered European air traffic due to hazards posed to aircraft intercepting the plume. The disruptions lasted 5 days, costing the aviation industry an estimated $250 million each day (Gudmundsson et al., 2010)

Monitoring volcanic emissions can give insight into the particular characteristics of a volcanic eruption, allowing for a better understanding of the associated hazards. Various geophysical techniques are useful in studying volcanic emissions and help provide insight into what drives and/or sustains an eruption. For example, concentrations of individual gases can be directly measured to infer the temperature and chemical composition of the magmatic reservoir (Aiuppa et al., 2002; Lambert et al., 1985). Remote sensing of CO_2 and SO_2 emissions from an eruption give insight into the depth of the magma body and other volcanic phenomena (Casadevall et al., 1994; Fischer, 2008; Werner et al., 2013). Volcanic tremor resulting from the movement of magmatic fluids within the crust, studied using seismometers, gives insight into volcanic emissions before they reach the surface (Aki et al., 1977; Chouet, 1985). Infrasound, or low frequency sound between ~0.02-20 Hz, has been proven useful in tracking temporal changes in volcanic plume dynamics such as volume outflux of emissions and eruption style (Fee and Matoza, 2013; Johnson and Ripepe, 2011).

I.2 Motivation for Infrasound Studies

Infrasound has proven useful in the analysis and detection of volcanic eruptions. Volcano infrasound studies have given insight into eruption dynamics, including eruption type and estimates of emissions (Fee and Matoza, 2013; Firstov, 1996; Johnson and Ripepe, 2011). Atmospheric perturbations from various volcanic processes often produce characteristic infrasound signals. Exsolution of gases can produce both short duration explosions and longer duration tremor. More violent, sustained eruptions produce signals characteristic of volcanic jets and plumes (Fee and Matoza, 2013).

It has been shown that different types of volcanic eruptions produce noticeably different infrasound signals (Fee and Matoza, 2013). Figure I.2.1 a-g shows examples of various infrasound signals produced by volcanoes. It is important to note that these eruptions differ in ash and gas content, viscosity of eruptive products, and other characteristics. While the differences in infrasound signals cannot yet be linked directly to individual eruption characteristics such as gas or ash content, the differences in overall shape of the signals are apparent. Fee and Matoza (2013) provide a comprehensive list of eruptive activity, general infrasound characteristics, and acoustic source processes in order to link differences in infrasound characteristics with differences in eruption type.

Volcano infrasound signals can be divided into three subcategories based on the distance signals are recorded from the source. Local infrasound, collected < 15 km from the eruptive source, is useful for investigating source processes due to its short propagation path and relatively low attenuation. Numerous studies have shown this through the use of source inversion methods, although complex source processes are still poorly understood. In cases with a "simple source", or a source "without any directional nature" (Lighthill, 1978) a monopole source inversion method can be used to estimate the volume and size of individual explosions (Dalton et al., 2010; Firstov and Kravchenko, 1996; Johnson et al., 2008). Kim et al. (2012) made use of a more complicated source model at Tungurahua Volcano, Ecuador and found reliable estimates of volume outfluxes from explosive events, showing promise for studying complex source processes using local infrasound.

The collection of regional and global infrasound data (collected 15-500 km and > 500 km from the source, respectively) was greatly improved by the establishment of the Comprehensive Nuclear-Test-Ban Treaty (CTBT). This treaty, formed by the United Nations in 1996, was created in order to ban nuclear weapons testing. The CTBT established the International Monitoring System (IMS), a global network of seismic, infrasound, hydroacoustic, and radionuclide sensors used to verify compliance with the treaty. Under preferential conditions, atmospheric waveguides and low attenuation allow infrasound to propagate far from the source, permitting global detection of large volcanic eruptions. The IMS network has proven particularly useful for the detection

and characterization of remote eruptions where other monitoring technologies are limited (Fee and Matoza, 2013). Regional infrasound from eruptions of Tungurahua Volcano was used to create an automated detection and notification system for volcanic hazards (Fee et al., 2010; Steffke et al., 2010). IMS arrays as far as ∼5000 km from the volcano collected infrasound during the 2008 eruption of Kasatochi Volcano in Alaska. These data allowed for investigation of infrasonic "jet noise", a newer area of research in the field (Fee et al., 2010).

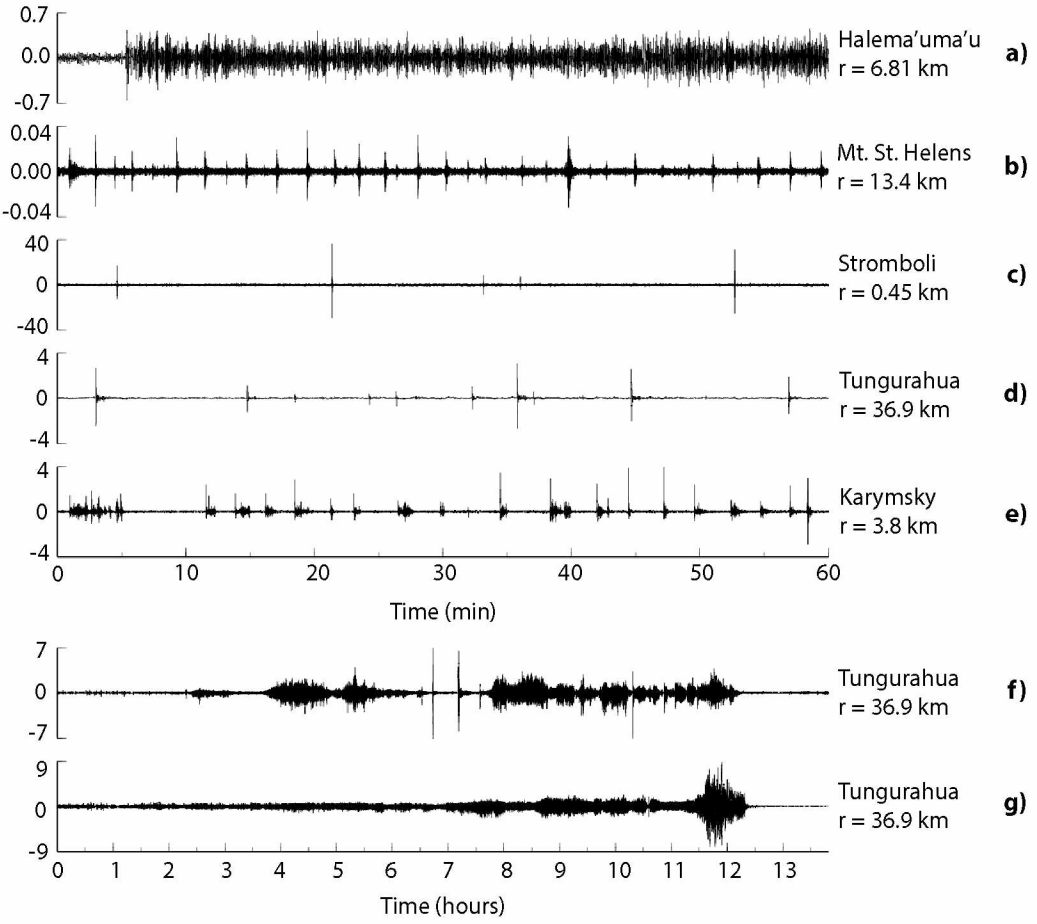

Figure I.2.1: Examples of various eruption types and their corresponding acoustic signals. The volcano and recording distance, r, are listed next to each plot. a) Acoustic tremor from the Halema'uma'u Vent, Kilauea Volcano, Hawaii. The initial blast corresponds to an impulsive explosion that cleared the vent. b) Infrasonic pulses recorded at Mt. St. Helens. Event durations are $\sim$10 s and have been correlated with seismic "drumbeat" events. c) Short-duration explosive events at Stromboli Volcano, Italy. d) Explosions followed by harmonic tremor at Tungurahua Volcano, Ecuador. e) Strombolian-like signals from Karymsky Volcano, Russia. These infrasound signals differ from typical Stombolian-type in their larger compression and smaller rarefaction. The longer duration of these explosions suggests volcanic jetting occurred. f) Another eruption at Tungurahua Volcano, but this one is subplinian in nature (i.e. larger than the eruption in d). Multiple pulses of longer-duration infrasound with large short-duration explosions occur. g) A larger, subplinian-plinian eruption of Tungurahua Volcano. Here the infrasound signal is sustained and gradually builds up to its highest pressure at hour 11.75. The height of the plinian phase lasts $\sim$45 minutes. It is important to note that f-g represent 14 hours of data while a-e represent 1 hr of data. (Fee and Matoza, 2013).

I.3 Thesis Work

This thesis presents one main body of research and suggestions for future work that effectively provide insights into eruption dynamics at various volcanoes. The main body of research focuses on the 2012-2013 eruption of Tolbachik Volcano. Strombolian-type activity, or frequent short-duration explosions, characterized this eruption. These short-duration explosions occur from large gas bubbles that rise through the volcanic conduit. The bubbles expand as they rise, reach the surface of a lava lake, and then burst to create explosions. Four sets of infrasound data were collected during the eruption. These consist of single sensor data collected February 12-14, 2013 and three-sensor data collected August 14-19, 2013 though not continuously, resulting in three data segments. Multi-sensor data in August allows for comparison of various explosion-picking methods in order to gain accuracy in analyses. Upon identifying explosions, a well-established method is implemented to estimate total volume of emissions from each individual explosion. From these calculations, three possible scenarios are presented for the eruption dynamics at Tolbachik Volcano from mid-February to late August 2013: the first being that the eruption stays consistent through time, the second representing a transition from larger explosions in February to a mixture of smaller and larger explosions in August, and the third representing a transition from larger explosions in February to a mixture of smaller and larger explosions in August, but with fewer explosions overall. Regional infrasound data are used to investigate eruptive intensity near the beginning of the Tolbachik eruption as no local data are available. Particularly noticeable in the regional infrasound data is the absence of an infrasound signal on November 27, 2012, the presumed onset (Gordeev et al., 2013; Zelenski et al., 2014). The appearance of infrasound about a day later suggests an increase in eruptive intensity occurred on November 28-29, 2012. Chapter 1 provides the submitted manuscript that further details this work.

Additional results and suggestions for future work are presented in the Conclusions section. The additional analysis focuses on local infrasound data collected at Karymsky and Sakurajima Volcanoes. Both of these volcanoes range in volcanic activity from discrete, short-duration ash- and gas-rich explosions to longer-duration, ash-rich explosions. Infrasound data collected at Karymsky Volcano in August 2011 are complemented by concurrent gas data and thermal imagery of the explosions. The variation in eruptive styles at both volcanoes makes the multiparameter dataset from Karymsky particularly useful in understanding how eruption characteristics affect acoustic waveforms. Eruption characteristics, such as relative concentration of gas vs. ash, general plume characteristics, plume altitude above the vent, plume temperature, and SO_2 emission rates likely play a role in affecting the shape of the acoustic waveform resulting from an eruption. We find that waveform shape can be roughly correlated to eruption characteristics at Karymsky Volcano in Kamchatka, Russia. The Conclusions section presents these promising results and offers ideas for future work.

Understanding volcanic emissions results in better preparedness for the associated hazards posed to humans, livestock, vegetation, and aircraft. Various methods can be used to study these emissions, including ground-based sampling of ash and pyroclasts, remote sensing for temperature and gas, and seismic, geodetic, and infrasound observations. Of these methods, infrasound is particularly promising because of its source generation location within the shallow conduit or just above the vent. The source location allows for infrasound observations to be directly correlated with both direct and remote observations of volcanic emissions produced at the vent (Fee and Matoza, 2013). This thesis presents current research and suggestions for future work on volcano infrasound that investigate volcanic eruption dynamics at three volcanoes.

Chapter 1 Infrasound from the 2012-2013 Plosky Tolbachik, Kamchatka Fissure Eruption[3]

1.1 Introduction

Infrasound, or low frequency sound between ~0.02-20 Hz, has proven useful in the analysis and detection of volcanic eruptions. Volcano infrasound studies have given insight into eruption dynamics, including eruption type and estimates of emissions (Fee and Matoza, 2013; Firstov, 1996; Johnson and Ripepe, 2011). It is well known that atmospheric perturbations from various volcanic processes can produce characteristic infrasound signals. Exsolution of gases can produce both short duration explosions and longer duration tremor. More violent eruptions produce signals characteristic of volcanic jets and plumes (Fee and Matoza, 2013).

Local infrasound (collected <15 km from the source) and seismicity from short duration explosions have been studied extensively at various volcanoes including Sakurajima and Unzen Volcanoes in Japan (Garces et al., 1999; Yamasato, 1998), Soufriere Hills Volcano, Montserrat (Green and Neuberg, 2005), Mt. Etna, Italy (Gresta et al., 2004; Ulivieri et al., 2013), Arenal Volcano, Costa Rica (Hagerty et al., 2000), Mt. Erebus, Antarctica (Johnson et al., 2008), Shishaldin Volcano, Alaska (Petersen and McNutt, 2007; Vergniolle et al., 2004), and Tungurahua Volcano, Ecuador (Kim et al., 2012; Ruiz et al., 2006). Some of these short duration explosions are the result of gas slug bursts. It was originally proposed that an explosion may occur when a bubble rises through the conduit and quickly undergoes expansion once it reaches a lower density zone (Buckingham and Garces, 1996). Additional infrasound-derived slug burst explosion models involve a rising gas slug oscillating at the surface of the lava lake and then bursting (Brandeis et al., 1994). While infrasound signals from slug bursts do vary, the typical impulse-like signal of an explosion consists of a compression (a wave which provides a large increase in pressure) followed by an almost equal rarefaction (an area of low pressure which follows). Similar slug burst events occurred during the recent 2012-2013 eruption of Tolbachik Volcano in Kamchatka, Russia.

Along with local infrasound from an eruption, regional infrasound data (collected ~15-500 km from the source) can be used to track changes in eruptive activity through time (Fee and Matoza, 2013). The Comprehensive Nuclear-Test-Ban Treaty (CTBT) was designed by the United Nations in 1996 to ban nuclear weapons testing and in turn created the International Monitoring System (IMS). The global IMS network consists of seismic, infrasound, hydroacoustic, and radionuclide sensors. Under preferential conditions, atmospheric waveguides and low attenuation allows infrasound to propagate far from the source, thus permitting global detection of volcanic eruptions using the IMS infrasound network. This network has proven particularly useful for the detection

[3]Chapter 1 is intended for publication in the Journal of Volcanology and Geothermal Research and has already been submitted to the journal. It is presented here under the knowledge and approval of co-authors.

and characterization of remote eruptions (Fee and Matoza, 2013). One of the IMS infrasound arrays, IS44, is located in Kamchatka, Russia ~384 km south of Tolbachik Volcano (Fig. 1.1.1a). This array recorded infrasound signals near the onset time of the 20122013 eruption of Tolbachik Volcano.

In this manuscript we use local and regional infrasound data to gain insight into the eruption dynamics of Tolbachik Volcano. Data collected at the IMS array in Kamchatka, Russia provides constraints on the eruption onset. The presence or absence of an eruption signal at the regional infrasound array helps give insight into how energetic the eruption was in late November 2012. Local infrasound sensors, deployed hundreds of meters from the active vent in February and August 2013, recorded frequent, repetitive explosions. These repetitive explosions are assumed to be a result of near-continuous bursting of large gas slugs. The volume outflux from each gas slug burst can provide insight into the eruption size and how it changes through time. The nature of these gas slug bursts allows for the assumption of a "simple source", or a source "without any directional nature" (Lighthill, 1978). This type of source radiates pressure equally in all directions and is known as an acoustic monopole. Estimates of individual gas slug volume and size can be calculated when an acoustic monopole source model is assumed (Dalton et al., 2010; Firstov and Kravchenko, 1996; Johnson et al., 2008). By using the acoustic data acquired from this eruption we 1) explore the adequacy of slug burst event-picking methods, 2) estimate the total volume outflux of emissions and the slug radius for each event, and 3) identify any temporal changes in both the local and regional infrasound in order to better understand the dynamics of this particular eruption.

1.2 Tolbachik Volcano

The Tolbachik Volcanic complex, created 40,000-50,000 years ago, consists of two volcanoes: Ostry Tolbachik, a stratovolcano creating the highest peak, and Plosky Tolbachik, a shield volcano that lies east of the summit (Fedotov et al., 2011). Currently, only Plosky Tolbachik is active and is referred to as Tolbachik Volcano or Tolbachik in this paper, as it is commonly referred. Tolbachik Volcano lies 3,085 m above sea level and is characterized by a summit caldera ~3.5 km in diameter. There are two zones of cinder cones, which formed 10,000 years ago. These zones reach out 20 km to the northwest and 50 km to the southwest of the volcanos summit. The magmatic plumbing system stems from the Klyuchevskoy Volcano Group and is characterized by a magma chamber that lies directly below Tolbachik Volcano at a depth of ~2 km and with a volume of 40-70 km^3 (Fedotov et al., 2011).

The most recent activity at Tolbachik Volcano is characterized by large eruptions in 1941, 1975-76, and 2012-13. The 1975-76 eruption was very large, being referred to as The Great Tolbachik Fissure Eruption. It began in late June 1975 as weak explosions from the summit crater.

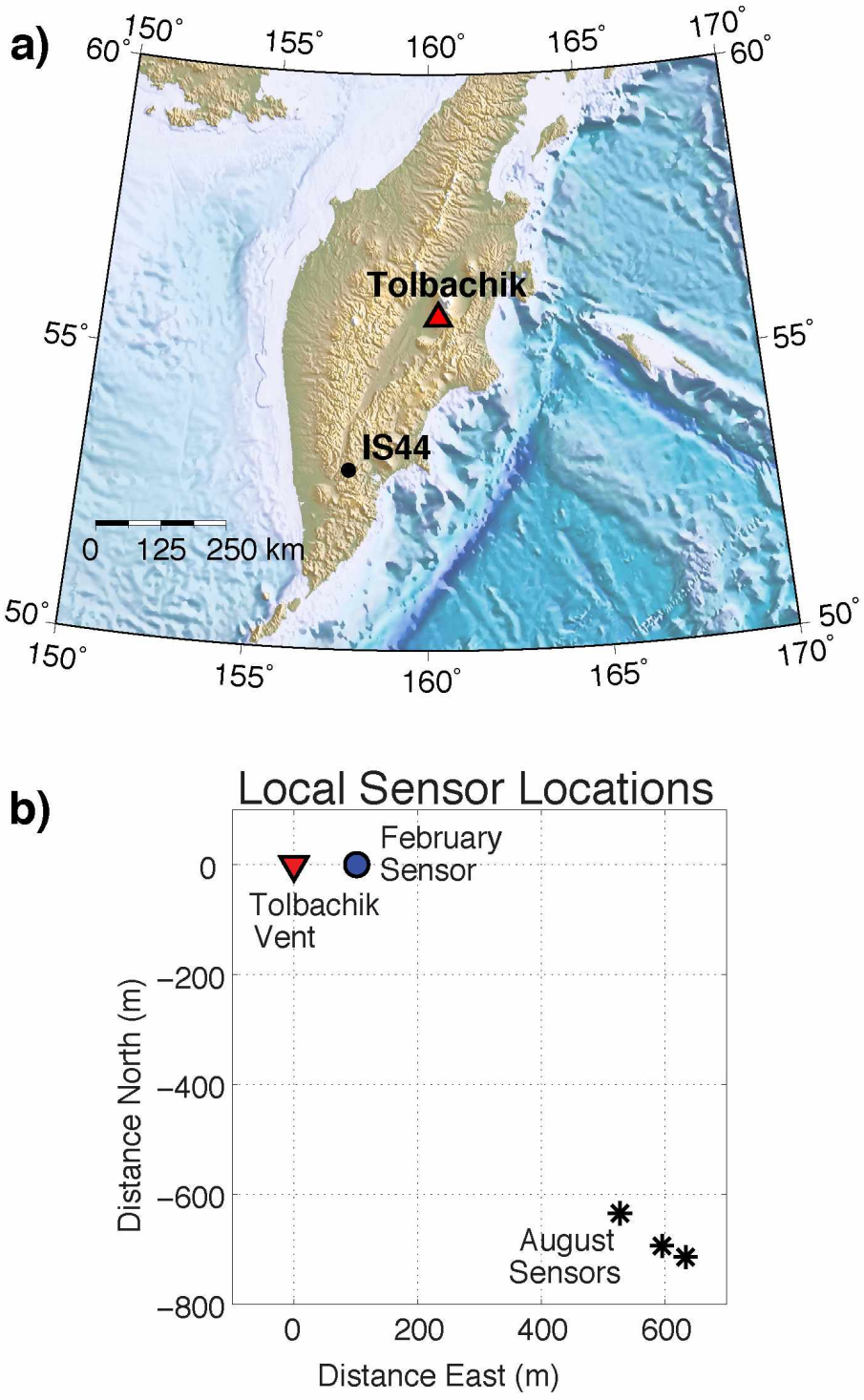

Figure 1.1.1: Study area location. Locations of a) Tolbachik Volcano and the International Monitoring Station IS44 infrasound array in Kamchatka, Russia and b) local sensors in February and August 2013 in reference to the active vent.

Just over a week later, three cones began to form north of the summit along with fissure activity. Activity lasted ~72 days, producing a total erupted volume of 1.18 km^3, consisting of tephra deposits and lavas. Eruptive activity north of the summit was similar to the activity that occurred in 1941 (Braitseva et al., 1997; Fedotov et al., 2011; Inbar et al., 2011). During the 1975-76 eruption, a cone also formed south of the volcano's summit. Weak Strombolian-type activity at the southern cone, superimposed on the continuous effusive activity, lasted for ~450 days. This single cone produced 0.968 km^3 of lava (Fedotov et al., 2011; Inbar et al., 2011). The 2012-2013 eruption of Tolbachik Volcano was no exception to the historical activity. It began as a fissure eruption at 5:15 UTC on November 27, 2012 and continued into late September 2013, though most of the activity occurred before August 24, 2013 (Gordeev et al., 2013; Zelenski et al., 2014). After a few days the fissure eruption transitioned to a discrete vent along the volcano's flanks. By December the eruption had largely transitioned to a second discrete vent where Strombolian activity dominated. Each vent produced a lava flow. By December 13, 2012, Gordeev et al. (2013) estimate volumes of erupted lavas from both vents to be 0.0207 km^3 and 0.208 km^3, respectively. During the eruption a lava lake was also present in the crater. Slug bursts were frequent within the lava lake (Gordeev et al., 2013; Zelenski et al., 2014). Preliminary calculations by Firstov et al. (personal communication, March 1, 2015) estimate the average mass outflux of emissions from slug bursts in February 2012 was ~250 kg/s. During this time, visual observations suggest explosions occurred every 3-5 seconds on average.

1.3 Data

1.3.1 Local Infrasound

In collaboration with the Kamchatka Branch Geophysical Surveys (KBGS) and Institute of Volcanology and Seismology (IVS), a single National Center for Physical Acoustics (NCPA) infrasound sensor placed ~100 m from the active vent collected data from February 12-14, 2013 (Fig. 1.1.1b). This sensor uses piezo-ceramic sensing elements with a 24-bit digitizer. Timing is given by Global Positioning System. The sensors have a flat frequency response between ~0.02-250 Hz and can reach pressures of ±1190 Pa. Three Hakusan Corporation infrasound sensors (models SI102 and SI103) located ~825-955 m from the vent collected data from August 14-20, 2013, though not continuously (Fig. 1.1.1b). Both Hakusan Co. models have a flat frequency response between ~0.1-1000 Hz. During both deployments a lava lake was present in the active crater. Slug bursts occurred in the lava lake and are confirmed by video data collected Feb. 12-14, by visual observations (Fig. 1.4.1), and are seen in the infrasound data by their characteristic shape (Fig. 1.4.2). Local infrasound data shows repetitive bursts occurring frequently with varying amplitudes (Fig. 1.4.2). Similarities are present between this data and acoustic signals from Mt. Etna in 2006-2013 (Ulivieri et al., 2013). During this period, Mt. Etna produced repetitive explosions similar to those occurring at Tolbachik Volcano in mid-February and late August 2013, but with much higher amplitudes.

These repetitive explosions are assumed to be the result of near-continuous gas slug bursts.

Our data and analyses are primarily limited by single sensor data in February and noise contamination in the form of roiling within the lava lake in August. Therefore, it was necessary to explore various filtering and cross correlation methods to extract information on the eruption dynamics. We experimented with band-pass and high-pass filtering methods and examined cross correlation values between sensors in three August datasets. A windowed cross correlation method was implemented to find events in the August data using a master waveform. These methods are further detailed in Section 1.4.1.

1.3.2 Regional Infrasound

Regional data were recorded by the IMS array, IS44, located in southern Kamchatka, Russia (Fig. 1.1.1a). IS44 is located ~384 km to the southwest of Tolbachik Volcano. The array recorded continuous data before the eruption, during the eruption from November 27, 2012 through September 2013, and after September 2013. This manuscript, however, focuses on only the data collected at the IS44 array during the first few days of the Tolbachik eruption, November 27-30, 2012. The IMS data are contaminated by wind so the pure-state filter is employed to remove noise (Olson, 2004). Usage of the pure-state filter is further detailed in section 1.4.3.

1.4 Methods

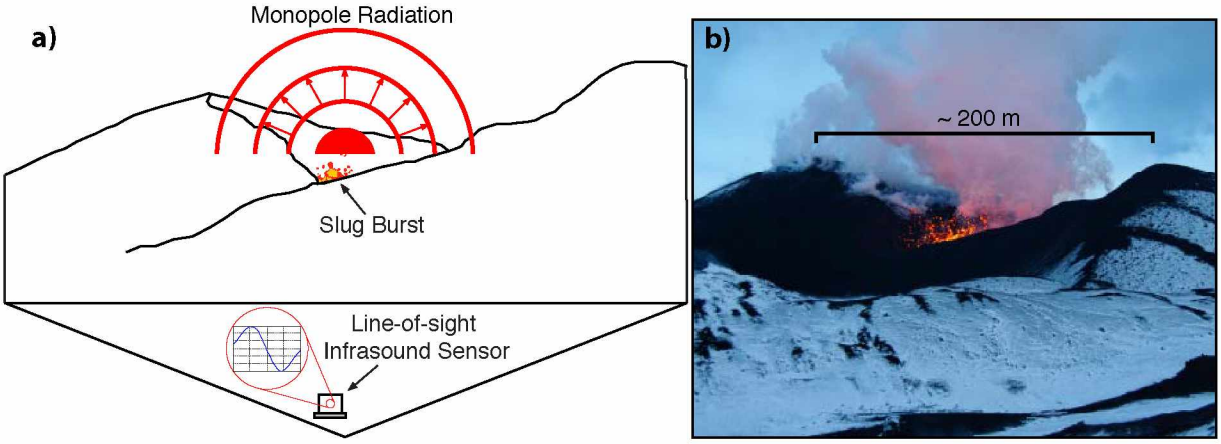

Figure 1.4.1: Tolbachik's active vent. a) Monopole point source model and radiation pattern. The slug burst acts as a point source from which acoustic waves radiate equally in all directions. The line-of-sight infrasound sensor allows for direct collection of waveforms from the source. Slug burst explosions create simple, sinusoidal, waveforms as shown in the circle emanating from the sensor. b) A picture of a slug burst occurring at the active vent in February 2013.

1.4.1 Explosion Picking Methods

We explore multiple methods to detect slug burst events. The repetitive nature and similarity of the explosions allowed for the use of a windowed cross correlation (WXC) method to pick explosions from a ∼1 second "master" waveform, chosen to isolate explosive events in each dataset (Anstey, 1964; Petersen, 2007; Petersen and McNutt, 2007). The master waveform is chosen to be characteristic of the explosion data in that it exhibits the typical compression and rarefaction signals of a slug burst (Fig. 1.4.1a, 1.4.2). The master waveform is then cross-correlated across the data in 1 second windows with 50% overlap. The short time window is necessary to capture individual events. Windows that produced a cross correlation value of 0.9 or greater are chosen as slug burst events from Tolbachik Volcano. The February data included video and visual observations, which aided in identifying a master waveform for a typical slug burst. The August data did not have accompanying video data, therefore a waveform with a high correlation value between all three sensors was chosen as the master.

Due to the availability of three-sensor data in the three August 2013 data, two filtering methods were employed in event-picking and sensor cross correlation. Data was first delayed based on the speed of sound and the distance from source to sensor. The speed of sound was determined by the highest signal power from delay and sum beamforming. For the first filtering method, we chose to band-pass filter the data between 0.55 Hz in order to avoid signal contamination from the microbarom (∼0.2 Hz signals that occur from natural processes related to ocean waves) (Donn and Rind, 1972). A high-pass filter (>5 Hz) was also experimented with due to the increased signal-to-noise ratio of slug bursts at higher frequencies. After filtering the data, windowed cross correlation was performed across all three sensors using a ∼1 second window with 50% overlap. The August data did not have accompanying video data, therefore a waveform with a high correlation value between all three sensors was chosen as the master. Windows that produced a mean cross correlation value of 0.9 or greater are chosen as slug burst events. For the duration of this paper these filtering and explosion picking methods will be referred to as the BPSC (Band-pass Filter and Sensor Cross Correlation) and HPSC (High-pass Filter and Sensor Cross Correlation) methods. It is important to note that the BPSC and HPSC methods are unique to the three August data because of the availability of three-sensor data.

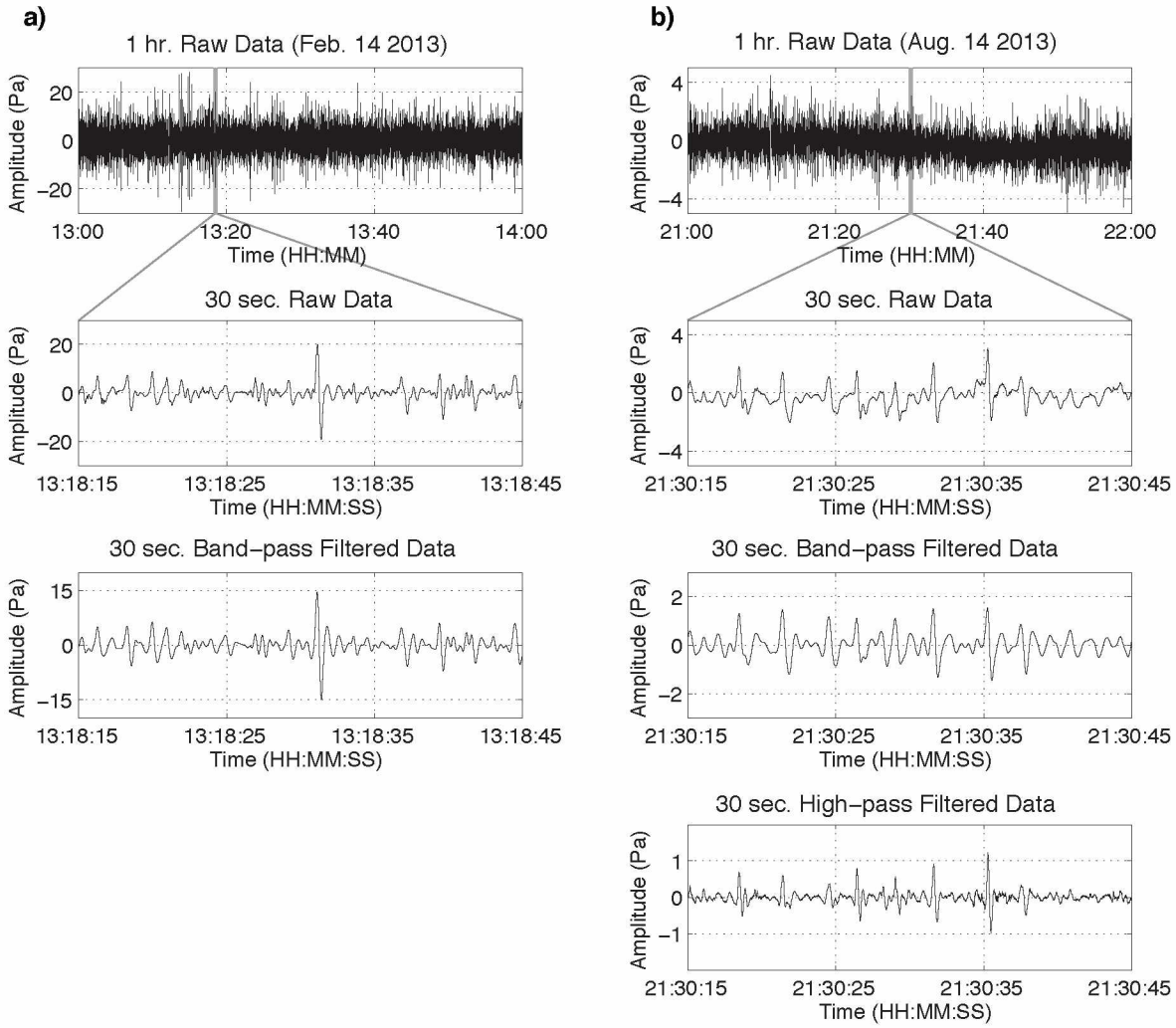

Figure 1.4.2: Sample of raw and filtered infrasound data recorded a) February 14, 2013 and b) August 14, 2013. Data are characterized by frequent slug burst events that produce repeated short-duration infrasound signals. 1 hour segments of raw data for both February and August are characterized by many short duration events. 30 second raw and filtered samples of data show events that display the characteristic shape of slug bursts with varying amplitudes. Band-pass filtering data for February makes slug burst events more evident. Both band-pass and high-pass filtering data in August makes slug burst events more evident.

1.4.2 Monopole Source Modeling

During February and August 2013, explosions from Tolbachik Volcano's discrete vent generally produced simple, impulsive, signals (Fig. 1.4.2). These signals were a product of atmospheric acceleration and can be likened to the bursting of a spherical balloon or a "symmetric chemical explosion" (Johnson et al., 2008). Figure 1.4.1 shows a schematic of the slug burst process and

the expected acoustic waveform. The simplicity of the waveforms and the assumed source process (repeated slug bursts) makes a monopole source model particularly fitting for our analysis (Dalton et al., 2010; Firstov and Kravchenko, 1996; Johnson et al., 2003, 2008). In some volcanic contexts the acoustic radiation from an eruption is not completely defined by a monopole source, but rather a combination of monopole and dipole sources. Kim et al. (2012) made use of this "multipole" source model at Tungurahua Volcano, Ecuador and found reliable estimates of volume outfluxes from explosive events with high signal-to-noise ratios. Explosions at Tungurahua Volcano are larger and more complex than the activity described in our study. Therefore, we assume that the eruptive source contains only a monopole component due to the simple nature of the slug burst events at Tolbachik Volcano. The far-field excess pressure radiated by a monopole source is given by the equation:

$$p - p_0 = \frac{\dot{q}(\tau - r/c)}{4\pi r} \tag{1.4.1}$$

where $p - p_0$ represents the excess pressure recorded by the acoustic sensor, $\dot{q}(t - r/c)$ represents the first derivative of the mass outflux (also known as the monopole source strength) at time $t - r/c$, r is the distance from the source to the sensor, and c is the speed of sound ($\sim$0.344 km/s) (Lighthill, 1978). For our experiment the speed of sound is determined from delay-and-sum beamforming for the highest signal power in August 2013. The volcanic context does not allow for complete spherical pressure radiation because of the Earth's surface. Therefore, a half space model is employed (using only half of the sphere) and the denominator of the monopole equation becomes $2\pi r$. From Equation (1.4.1), it is easy to see that the source strength, $\dot{q}$, can be solved for directly from the acoustic data. $\dot{q}$ (kg/s^2) is then integrated once to find the mass outflux (kg/s) and then again to find the cumulative mass outflux (kg).

It is perhaps easier to visualize the amount of emissions from each explosion as volume outflux rather than as cumulative mass outflux. Total volume outflux of emissions can be related to the cumulative mass outflux by the following equation:

$$Q = \frac{1}{\rho_{\text{air}}} S(t) \tag{1.4.2}$$

where Q is total volume outflux, $\rho_{\text{air}} = 1.14$ kg/m^3 (at 1500 m above sea level and 20 degrees C), and $S(t)$ is cumulative mass outflux for a particular explosion (Kim et al., 2012). Cumulative mass outfluxes were converted to total emissions volumes for each explosion and the equation for the volume of a sphere was employed to solve for the individual slug radius, assuming the slug exploded as a spherical bubble (Dalton et al., 2010; Johnson et al., 2008).

1.4.3 Regional Infrasound Analysis

Regional infrasound are analyzed between November 27-30, 2012. The data were first band-pass filtered between 0.5-5 Hz in order to remove microbarom effects. Upon band-pass filtering the data, the pure-state filter was employed to reduce background noise. This filtering method was chosen because of its effectiveness in filtering isotropic, uncorrelated, noise usually seen in infrasound array data. The spectral matrix from the data (the outer product of the Fourier transform of the time series data and its Hermitian conjugate) is used to estimate the degree of polarization, or "generalized coherence". Data with a high degree of polarization, P^2, are treated as coherent and are unperturbed by the filter. In turn, frequencies with a low P^2 value, or those characterized by noise, are suppressed (Olson, 2004).

After filtering, signal back-azimuths and trace velocities as well as a measure of signal-to-noise ratio (Fisher Statistic) were calculated in order to find infrasound signals from Tolbachik Volcano. Least squares estimation was implemented to find the back-azimuths and trace velocities of plane wave acoustic signals traversing the array in 20 s windows with 50% overlap (Szuberla and Olson, 2004). The Fisher Statistic (F-statistic) was used to give a measure of the signal-to-noise ratio (SNR) and was also computed for each 20 second window. The F-statistic is related to the SNR by $\mathrm{SNR} = ((F - statistic - 1))/N$, where N is the number of samples (Blandford, 1974). A SNR threshold of 1 (i.e. $\mathrm{F} > 5$), back-azimuth of 27 ± 8 degrees, and trace velocity of 0.34 ± 0.10 km/s were used in order to identify time windows with signals originating from Tolbachik Volcano.

1.5 Results

1.5.1 Comparison of Explosion-Picking Methods

The WXC, BPSC, and HPSC methods were experimented with in order to identify slug burst events within the three August datasets, and to examine the adequacy of the WXC method used in the February dataset. Figure 1.5.1 shows a comparison of probability density functions (PDFs) of the selected waveforms for the February data and each of the August datasets using each filtering method. The beginning date of each dataset and the explosion picking methods are denoted in the title of each plot. The numbers in each plot correspond to the cross correlation value between the highest probability line (white dashed line) and the master waveform (black dashed line) used in the WXC method for that data. 95% confidence intervals for the waveform probability densities are shown as grey lines. The master waveforms from the WXC method are plotted as a reference of how well the highest probability matches an actual event. Amplitudes are normalized.

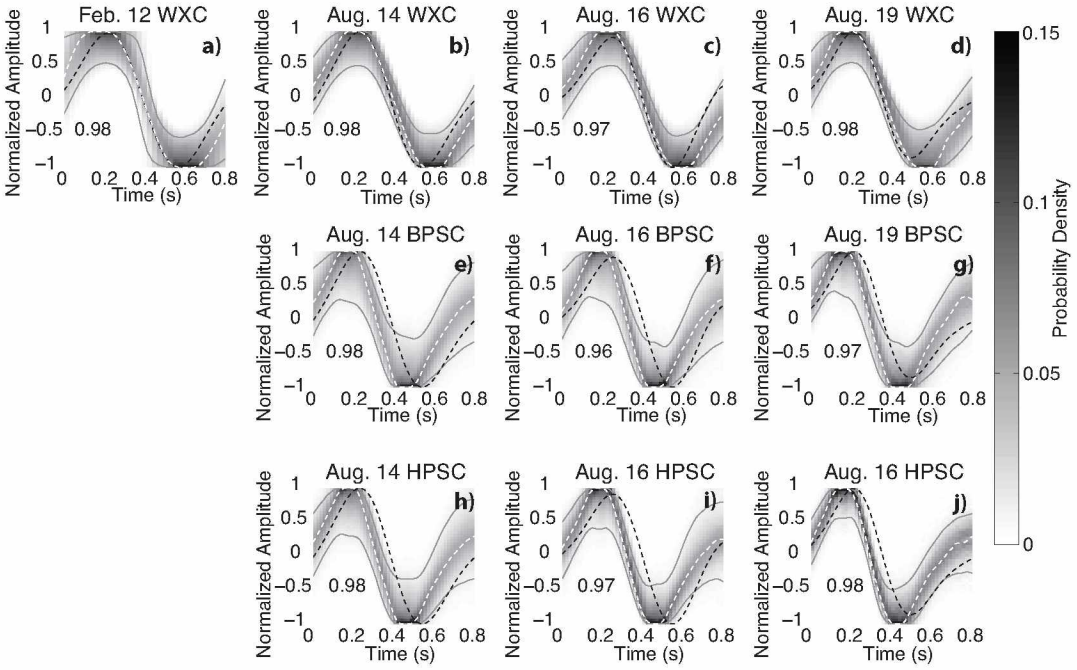

Figure 1.5.1: Comparison of probability density functions (PDFs) of the selected waveforms for each data set and explosion-picking method. The beginning date of each dataset and the explosion picking methods are denoted in the title of each plot. The numbers in each plot correspond to the cross correlation value between the highest probability line (white dashed line) and the master waveform (black dashed line) used in the WXC method for that data. 95% confidence intervals for the waveform probability densities are shown as grey lines. Amplitudes are normalized. The highest probabilities derived from each PDF both qualitatively and quantitatively match their corresponding WXC master waveforms well.

1.5.2 Total Emissions Values

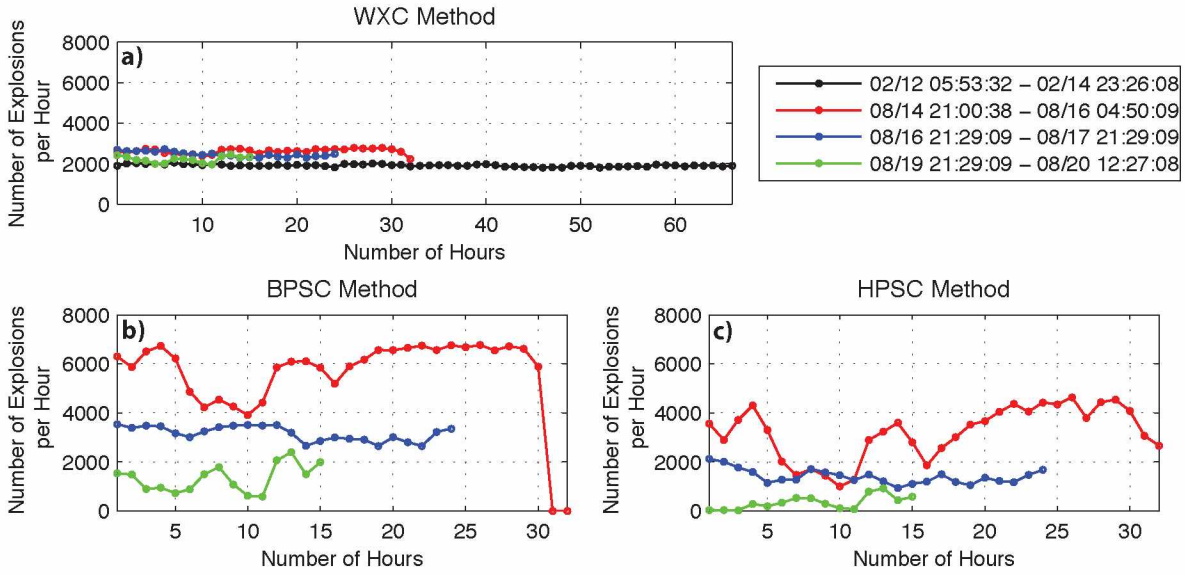

Figure 1.5.2: Number of explosions per hour for datasets using the following methods: a) WXC, b) BPSC, and c) HPSC. The WXC method shows a relatively consistent trend for all datasets. The BPSC and HPSC methods show noticeable decreases in number of explosions per hour for the August 1620 datasets. Table 1 provides a comprehensive list of the average number of explosions per hour and the recurrence intervals for each data set and method.

We now investigate the timing between slug burst events. Video observations made ~100 m from the vent in February give estimates that slug burst explosions occurred every 3-5 seconds. The WXC method suggests an average number of ~1910 explosions per hour, which translates into a recurrence interval of 1.9 seconds per explosion (Fig. 1.5.2). The three methods employed in the August data show average number of explosions per hour ranging from 345-5560, or recurrence intervals ranging from every 0.6 s up to every 10 s depending on the method (Fig. 1.5.2). The number of events per hour stays relatively consistent for all four datasets when the WXC method is employed (Fig. 1.5.2a). Both the BPSC and HPSC methods show noticeable variations (Fig. 1.5.2b-c). The WXC method shows the most consistency with on average 1910, 2610, 2470, and 2210 explosions per hour (every 1.9 s, 1.4 s, 1.5 s, and 1.6 s) for the data beginning February 12, August 14, August 16, and August 19 respectively. The highest variance for the average number of explosions occurring per hour results from the HPSC method. This method gives average values of 3190, 1400, 345 explosions per hour (every 1.1 s, 2.6 s, and 10 s) for the data beginning on August 14, August 16, and August 19. The BPSC method gives average values of 5560, 3160, and 1330 explosions per hour, or every 0.6 s, 1.1 s, and 2.7 s for the data beginning August 14, August 16, and August 19 respectively A comprehensive list of total number of explosions, average

number of explosions per hour, and average recurrence intervals per hour is displayed in Table 1.5.1.

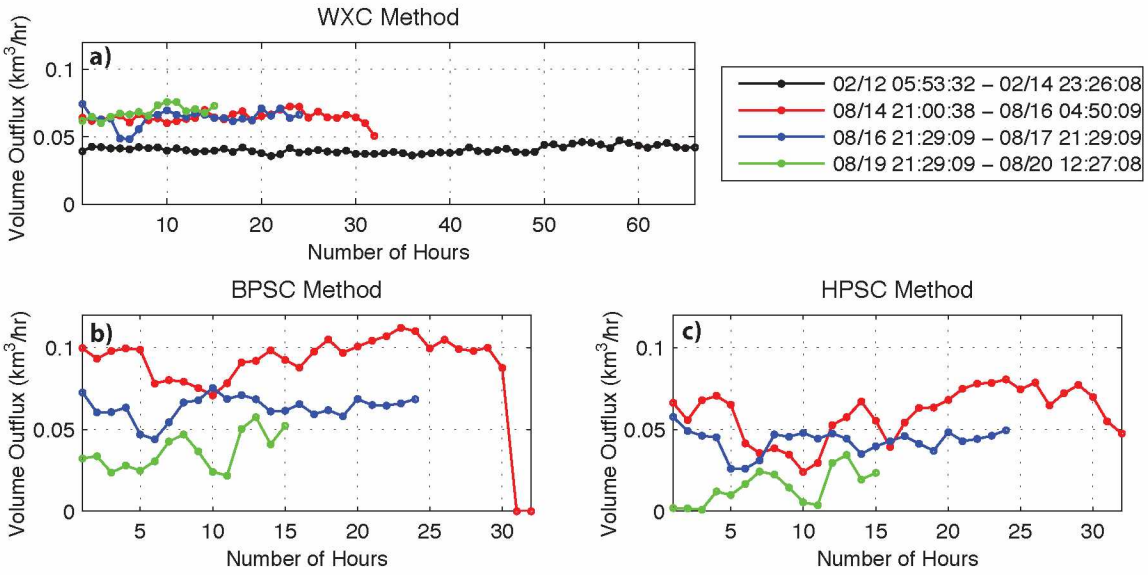

Figure 1.5.3: Total volume outflux of emissions per hour using the following methods: a) WXC, b) BPSC, and c) HPSC. As in Figure 5, the WXC method shows a relatively consistent trend for all datasets, whereas the BPSC and HPSC methods show noticeable decreases in total volume outflux per hour for the August 1620 datasets. Table 1 provides a comprehensive list of the total volume outflux per hour for each dataset and method.

We now estimate the total volume outflux of emissions and solve for gas slug radius for each event found in the four datasets using the WXC, BPSC, and HPSC methods. Figure 1.5.3a shows the total volume outflux per hour from the events identified using the WXC method, while Figure 6b-c shows the same calculations using the BPSC and HPSC methods. Similar trends are present in the total volume outflux as in the number of explosions (Fig. 1.5.2, 1.5.3). When the WXC method is employed, the total volume outflux per event stays relatively stable for each dataset. The BPSC and HPSC methods show that the highest total volume outflux per hour generally results from the data beginning August 14, 2013 while the lowest total volume outflux per hour results from the data beginning August 19, 2013 (Fig. 1.5.3b-c). A comprehensive list of total volume outflux is displayed in Table 1.5.1.

Slug radii values were calculated for each event. Figure 1.5.4 shows the distribution of slug radii values for the three methods. In these plots the August data are represented by blue bars and have been grouped into one distribution because of their proximity in time. Even though the WXC method was the only method employed on the February data, the distribution of radii values are plotted as red bars in each plot for use as a reference. Radii values calculated from events

picked using the WXC method show a normal distribution with a mean of 3.36 m and 3.76 m for the February and August data respectively. The BPSC and HPSC methods produced many radii values that fall near zero. The smallest mean radii value for the August data comes out of the usage of the BPSC method and is 2.77 m. The HPSC method falls in the middle, giving a mean slug radii size of 3.51 m. Table 1.5.1 provides a comprehensive list of the number of explosions, total volume outfluxes, mean slug radii values, and average number of explosions per hour for the February and August datasets and methods.

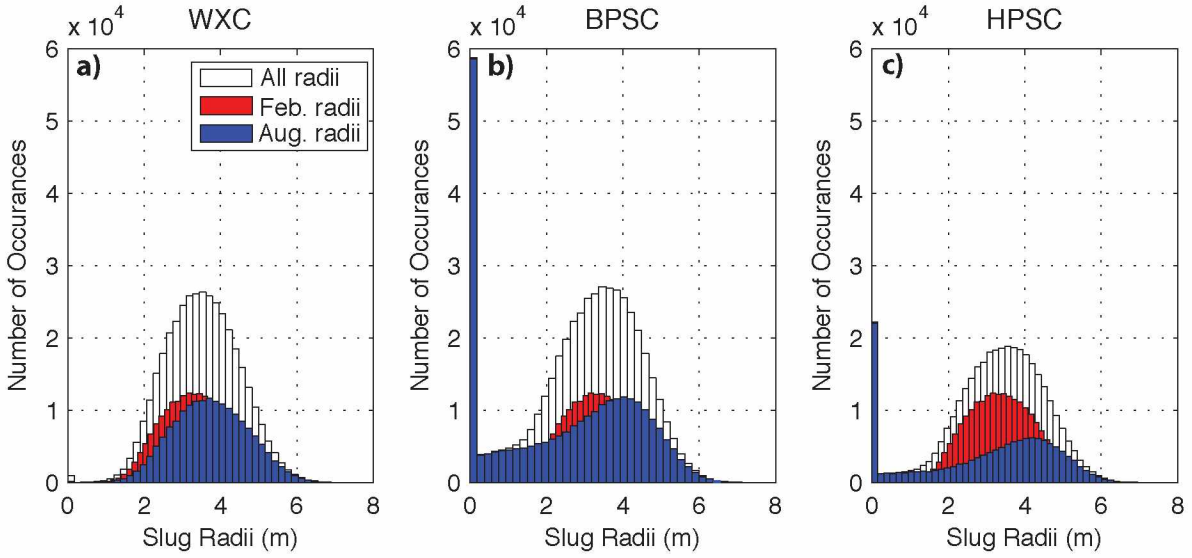

Figure 1.5.4: Slug radii distribution for the a) WXC, b) BPSC, and c) HPSC methods. The distribution of the total calculated radii for each method is displayed by the white bars. The distribution of the February radii values calculated from the WXC method are displayed by the red bars, while the August radii values calculated using the BPSC and HPSC methods are displayed in blue. August radii calculations have been grouped due to the proximity in time of the datasets. Radii values calculated from events picked using the WXC method show a normal distribution with a mean of 3.36 m and 3.76 m for the February and August datasets, respectively. The BPSC and HPSC methods produced many radii values that fall near zero. The smallest mean radii value for the August dataset originates from the BPSC method and is 2.77 m. The HPSC method falls in the middle, giving a mean slug radii of 3.51 m.

1.5.3 Results from Regional Infrasound

Array processing results from least squares and F-statistic analysis show numerous infrasound signals from Tolbachik Volcano detected at IS44 between November 28-29, 2012 (Fig. 1.5.5). It is known from seismic observations that the eruption began at approximately 05:15 UTC on November 27, 2012 and that the fissure eruption transitioned to a discrete vent within a few days (Gordeev et al., 2013; Zelenski et al., 2014). A trace velocity of 0.34 $\pm$ 0.1 km/s and a back azimuth of 27 $\pm$ 8 degrees is expected for signals from Tolbachik Volcano. No clear infrasound

arrivals are detected at IS44 on November 27 (Fig. 1.5.5). Therefore, the eruption onset cannot be seen in the regional infrasound data. However, signals with the correct trace velocities and back-azimuths for Tolbachik Volcano, as well as relatively high SNRs, are evident November 28 beginning around 00:00 UTC and continue into early November 29, 2012 (Fig. 1.5.5b-c). Filtered infrasound amplitudes during these periods are generally quite low (<0.1 Pa).

Table 1.5.1: Monopole calculations for windowed cross correlation, band-pass filter sensor correlation, and high-pass filter sensor correlation. August data have been grouped because of their nearness in time.

Data	Method	# of explosions	Average # of explosions per hour	Average recurrence interval (s)	Total volume outflux (km^3)	Average slug radius (m)
02/12 05:53:32 - 02/14 23:26:08	WXC	241,765	1913	1.9	0.033	3.36
08/14 21:00:38 - 08/16 04:50:09	WXC	83,776	2618	1.4	0.021	3.65
	BPSC	177,969	5562	0.6	0.028	2.45
	HPSC	102,209	3194	1.6	0.019	2.73
08/16 21:29:09 - 08/17 21:29:09	WXC	59,150	2465	1.5	0.015	3.71
	BPSC	75,824	3159	1.1	0.015	2.77
	HPSC	33,730	1405	2.7	0.010	3.63
08/19 21:29:09 - 08/20 12:27:08	WXC	33,217	2215	1.6	0.010	3.92
	BPSC	19,962	1331	2.6	0.0055	3.09
	HPSC	5,173	345	10.	0.0022	4.16

1.6 Discussion

1.6.1 Adequacy of Explosion Picking Methods

PDFs of events picked using all three methods (Fig. 1.5.1) generally show waveforms characteristic of slug bursts as suggested by their simple and sinusoidal shape. A compression and a relatively equal rarefaction can be seen in the highest probability lines. The highest probabilities derived from each PDF both qualitatively and quantitatively match their corresponding master or mean waveforms well. This can be seen in the very high cross correlation values present between the highest probability lines and the master or mean waveforms from each dataset (all above 0.95)

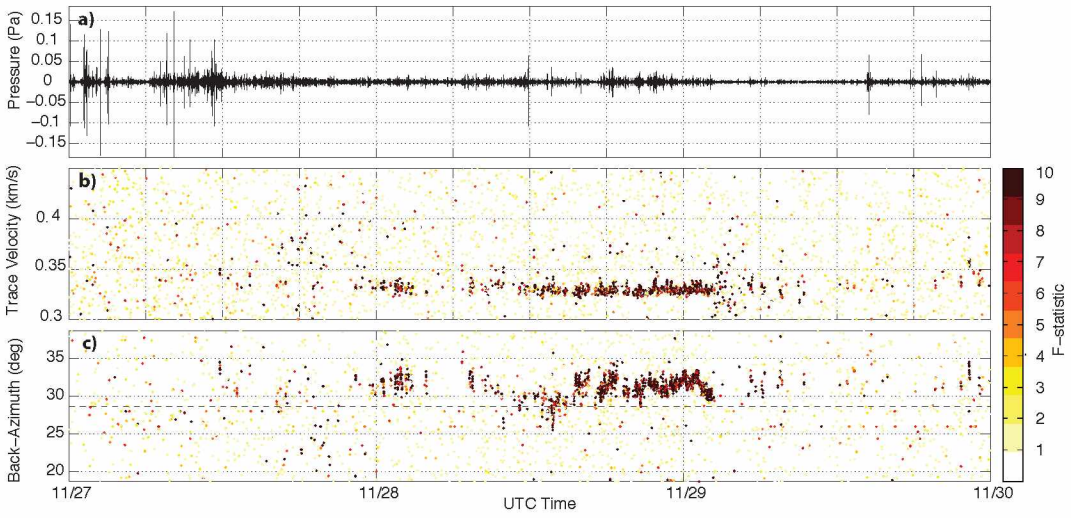

Figure 1.5.5: Regional infrasound analysis for 27-30 November 2012. a) Infrasound data from IS44 filtered using a pure-state filter (Olson, 2004). b) trace velocity and c) back-azimuth for 20 s windows. Data segments are colored by the F-statistic, a measure of the SNR. Lava flows occurred from two centers and ash emissions were occurring at Tolbachik Volcano during this period (Gordeev et al., 2013a). The high SNR at this time along with the back-azimuths and trace velocities suggest signals from Tolbachik Volcano were picked up at the IS44 array between November 28 00:00 early November 29. Late November 29 November 30 shows fewer events from Tolbachik Volcano. The lack of a signal at the eruption's onset (November 27 5:15 UTC) and after early November 29 suggests a smaller eruptive intensity during these times.

(Fig 1.5.1a-j). Also, all master or mean waveforms either entirely or almost entirely lie within the 95% confidence limits of the probability densities for each dataset and method. Qualitatively, it is easy to see a compression and a relatively equal rarefaction in the highest probability lines (Fig. 1.5.1a-j).

Possible sources of error in the explosion picking methods include the short window length and picking of non-slug burst events or other non-volcanic infrasound signals. A longer window length is usually preferable because it allows for the cross correlation of more information. However, the 1 second window length was necessary for identifying slug burst events due to the simplicity of the signal. In our study, non-slug burst events may be attributed to roiling within the lava lake, especially when using the BPSC and HPSC methods. Roiling of a lava lake degassing has been found to be a significant source of infrasound (Fee and Matoza, 2013).

Even though sources of error are possibly present, the high cross correlation values between the highest probability lines and the actual events suggest most events were identified correctly.

Both the BPSC and HPSC methods identify smaller events, as seen in the distribution of slug radii sizes. Due to the high cross correlation value between the sensors, we deduce that these small events may be related to roiling within the lava lake as a result of persistent degassing. Because of the likelihood that all events detected in the three methods are indeed actual volcanic degassing events, the next section explores three possible eruption styles from mid-February to late August 2013: 1) the eruption stays consistent through time, 2) the eruption transitions from dominantly slug bursts in February to a mixture of roiling within the lava lake and slug bursting in August, or 3) the eruption transitions from dominantly slug bursts in February to a mixture of roiling within the lava lake and slug bursting in August, but fewer explosions occur overall.

1.6.2 Eruption Characteristics Through Time

Regional infrasound analyses can give insight into eruption dynamics at the beginning of the eruption. Results from this study are particularly promising for regional infrasound interpretation between November 28 and early November 29, 2012. It is known from visual observations that lava flows occurred from two centers and ash emissions were occurring at Tolbachik Volcano during this period (Gordeev et al., 2013). The relatively high SNR at this time along with the back-azimuths and trace velocities suggest signals from Tolbachik Volcano were picked up at the IS44 array between November 28 00:00 - November 29 2:00 UTC. November 29-30 shows fewer events from Tolbachik Volcano.

The eruption onset time, derived from seismic observations, is not seen in our regional infrasound data. This suggests it was not energetic enough for acoustic signals to propagate large distances (Fee and Matoza, 2013). Because signals from Tolbachik Volcano are seen in the regional data on November 28 to early November 29, the eruption likely increased in intensity during this period. The eruptive intensity must have returned to lower levels on November 30 because the signal is no longer seen. While it is unlikely atmospheric effects changed significantly during this study period, future detailed acoustic propagation modeling could give more detailed information into signal propagation from the volcano to the infrasound array on November 27 and 30. However, current results provide evidence for an increase in eruptive intensity from November 28 to early November 29, 2012.

Of the three methods employed on the local infrasound data, the WXC method shows the least change through time. Data from the WXC method suggests the number of explosions per hour, the total volume of emissions, and the slug radii size stayed consistent from February to August (Fig. 1.5.2a, 1.5.3a, 1.5.4a). Thus, these results suggest there was no change in the eruption from mid February 2013 to late August 2013. However, video and other observations from February and August suggest the eruption did change significantly. Video data from February could only be

taken at a distance because of the large and frequent explosions. Even so, discrete, large, explosions can clearly be observed. Video from August could be taken from the edge of the vent and shows smaller slug bursts and roiling within the lava lake. The consistency in the number of explosions and total volume of emissions through time occurs because this method ignores other signals produced from the lava lake. Unlike the other BPSC and HPSC methods, the WXC method only searches for signals that resemble large slug burst events. Because this method shows consistency in radii sizes through time and only identifies large slug bursts, the WXC method likely underestimates the total volume outflux in all data, but serves as a lower bound.

Alternatively, the BPSC method shows numerous small amplitude events along with a larger number of slug burst explosions overall (Fig. 1.5.2b, 1.5.3b, 1.5.4b). It is likely these smaller events are related to the roiling of the lava lake. Assuming the monopole calculations serve as an adequate estimate, the number of explosions and total volume outflux per hour decreased rapidly between August 14-20, 2013 (Fig. 1.5.2b, 1.5.3b). Due to the numerous small amplitude events, this method suggests the eruption in February and August consisted of a mixture of small amplitude roiling of the lava lake and larger amplitude explosions from slug bursts.

The third method, HPSC, generally shows a smaller number of events occurred overall (Fig. 1.5.2c, 1.5.3c, 1.5.4c). Results suggest a trend similar to that which is seen when implementing the BPSC method. This method also suggests the number of explosions and total volume outflux per hour decreased rapidly between August 14-20, 2013. However, the HPSC method finds fewer events with radii near zero (Fig. 1.5.4c). Therefore, the results from the HPSC method suggest the eruption was a mixture of roiling within the lava lake and larger slug burst explosions, but fewer events occurred overall.

As mentioned above, video observations show that roiling of the lava lake occurred in late August. We suggest this roiling can be modeled assuming a monopole source because it is essentially a combination of small bubble bursts. However, the nature of monopole source inversion suggests that it is likely that all methods underestimate the total volume of emissions. They do, however, provide a lower bound on the eruption emissions during mid February and mid to late August.

1.6.3 Implications for Volume Flux Calculations

Infrasound-based inversions for volume flux using a monopole assumption have been commonly used, although a number of assumptions must typically be made. These include the assumption that the source radiates sound equally in all directions and that the sound travels as a plane-wave in a homogeneous half-space. The assumption that the sound radiates equally in all directions allows for the attenuation of acoustic amplitude as $1/r$ (where r is the distance from

source to sensor). This is generally an adequate assumption when studying local infrasound unless significant topography is present (Fee and Matoza, 2013). This 1/r attenuation is in (1.4.1) as part of the spherical acoustic radiation pattern. Figure 1.6.1a-c shows the WXC master waveforms and their corresponding mass and cumulative mass outfluxes from the February and August data. Since the sensor in February is located only ∼100 m from the vent and the August sensors are located ∼825-955 m from the vent, the amplitudes of events in August must be ∼8.3-9.5 times smaller than those in February (i.e. their maximum amplitude must be less than 1.55-1.80 Pa) in order to obtain a similar cumulative mass outflux. While the master waveform from the data beginning August 14, 2013 fits the 1/r spreading rule, the master waveforms from the data beginning August 16 and August 19, 2013 are clearly greater than 1.80 Pa. Therefore, the calculations for the master waveforms from August 16 and 19 give greater values for total cumulative outflux. This phenomenon could explain why greater total volume outflux per hour (Fig. 1.5.3a) and larger average slug radii (Table 1.5.1) are seen in the August data when using the WXC method. However, we are confident that monopole source inversion is an adequate method to provide lower bounds on estimates of volume outfluxes for our data. Therefore, we postulate that these larger amplitudes are due to local propagation effects, to the contribution of a non-monopole component during this period, or to a deviation from spherically symmetric radiation. However, understanding the local propagation effects, the contribution of a non-monopole component, and/or the radiation pattern requires a more robust infrasound sensor configuration.

Similar studies have been done at other volcanoes, including Mt. Erebus, Antarctica (Firstov and Kravchenko, 1996; Johnson et al., 2008, 2004), Pacaya Volcano, Guatemala (Dalton et al., 2010), and Mt. St. Helens, USA (Moran et al., 2008). Data collected at Mt. Erebus, Antarctica by Johnson et al. (2008) displays slug burst signals with slight variations from the typical signal. This variation is likely due to some horizontal directional component of the source mechanism. Even so, explosions at Mt. Erebus between January 6 - April 13, 2006 were modeled using a monopole source model and show the cumulative outflux values from each explosion ranged from <1000 kg to ∼20,000 kg, with a median value of 5,000 kg (Johnson et al., 2008). Results from Pacaya Volcano in 2010 produced smaller slug bursts that gave cumulative flux values ranging from 12 kg to 962 kg. Moran et al. (2008) also used a monopole source inversion method, but on a rockfall instead of a volcanic eruption. Results from the rockfall show a cumulative outflux of 7.5×10^6 kg, far larger than values calculated from the volcanic eruptions. Ranges in cumulative outflux values for individual slug bursts from our data are listed in Table 1.6.1. For all datasets and methods the Tolbachik slug bursts show a per event cumulative outflux range greater than that calculated from measurements at Pacaya, less than those calculated from measurements at Mt. Erebus, and far less than those calculated from a rockfall at Mt. St. Helens. From this, we determine the slug bursts at Tolbachik volcano during February and August 2013 must have been

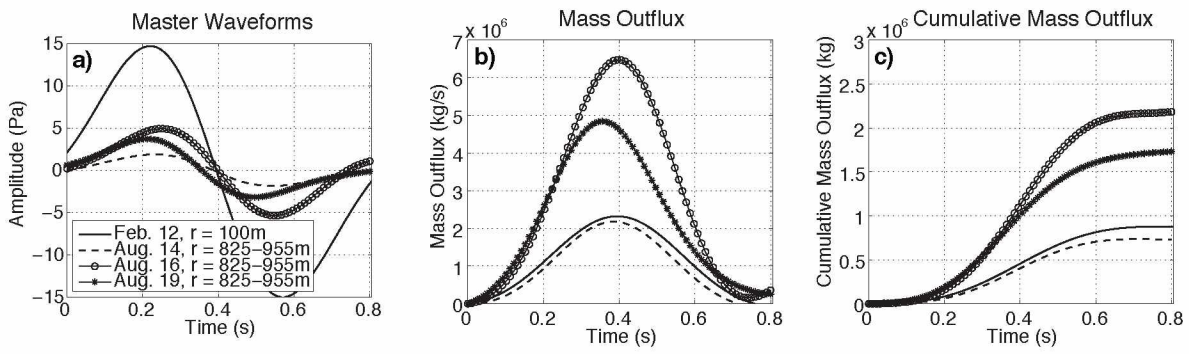

Figure 1.6.1: Infrasound-derived mass outflux calculations for the selected master waveforms. Plots show a) pressure traces of master waveforms from each dataset (noted by its distance, r, from the vent), b) corresponding mass outflux calculations, and c) cumulative mass outflux calculations. To obey the the 1/r spreading rule that describes the spherical acoustic radiation pattern based on distance from the source, the amplitudes of events in August must be ~8.3-9.5 times smaller than those in February (i.e. their maximum amplitude must be less than 1.55-1.8 Pa) in order to obtain a similar cumulative mass outflux. Only the dataset beginning August 14 has this relationship. This could explain why greater total volume outflux per hour and larger average slug radii are seen in the August data when using the WXC method. Larger amplitudes in the August data are possibly due to local propagation effects, the contribution of a non-monopole component, and/or a deviation from the assumed spherically symmetric acoustic radiation pattern.

larger on average than those at Pacaya Volcano in 2010, but smaller on average than those at Mt. Erebus in 2008.

1.7 Conclusions

Both regional and local infrasound data were analyzed to track and characterize the eruption dynamics of Tolbachik Volcano. Regional data focused on the eruption onset in late November 2012, while local data focused on eruptive activity in February and August 2013. Regional data gives insight into the intensity of the eruption from the presence or absence of the eruption signal. The eruption at Tolbachik Volcano was likely less energetic at the onset (November 27, 2012) and gained intensity at the time when it is first seen at the IS44 array (late November 28 - early November 29). After early November 29 the disappearance of the signal in the regional infrasound suggests that the eruption became less energetic once again. Three methods were employed to pick slug burst events from four local infrasound data, one in February and three in August. Each individual slug burst event was assumed to result from an acoustic monopole, allowing us to calculate the volume outflux and slug radius per event, as well as total volume outfluxes per hour for each dataset. Estimated emissions outfluxes and slug radii distributions provide three possible eruption styles for the eruption dynamics of Tolbachik Volcano from mid-February to late-August: 1) the eruption stays consistent through time, 2) the eruption transitions from dominantly slug bursts in

Table 1.6.1: Comparison of cumulative outflux values at various volcanoes.

Volcano (and/or method)	Range of cumulative outflux values (kg)
Mt. Erebus 01/06/06 - 04/13/06	$<$ 1000 - 20,000
Pacaya	12 - 962
Mt. St. Helens Rockfall	7.5×10^6
Tolbachik Total (Range of all data)	$<$ 100 - 3910
Tolbachik 02/12/13 05:53:32 - 02/14/13 23:26:08	$<$ 100 - 1539
Tolbachik 08/14/13 21:00:38 - 08/16/13 04:50:09	
WXC	$<$ 100 - 1805
BPSC	$<$ 100 - 1947
HPSC	$<$ 100 - 1802
Tolbachik 08/16/13 21:29:09 - 08/17/13 21:29:09	
WXC	$<$ 100 - 1847
BPSC	$<$ 100 - 2352
HPSC	$<$ 100 - 2352
Tolbachik 08/19/13 21:29:09 - 08/20/13 12:27:08	
WXC	$<$ 100 - 3048
BPSC	$<$ 100 - 3910
HPSC	$<$ 100 - 2072

February to a mixture of roiling within the lava lake and slug bursting in August and 3) the eruption transitions from dominantly slug bursts in February to a mixture of roiling within the lava lake and slug bursting in August, but fewer explosions occurring overall. The last two eruption styles most closely match visual observations. While emissions outfluxes from the WXC method likely underestimate the actual total emissions from Tolbachik Volcano during the study time periods, they do provide a lower bound. Cumulative outflux of emissions per event in both February and August range from <100 to ~3000 kg for all methods. These values are greater than emissions calculated at Pacaya Volcano, but less than those calculated from emissions at Mt. Erebus Volcano (Table 1.6.1). From this, it is determined that slug bursts at Tolbachik Volcano in February and August were larger on average than those at Pacaya Volcano in 2010, but smaller on average than those at Mt. Erebus in 2008.

Although the infrasound data collected from Tolbachik were adequate for the methods used in this paper, it is not unusual to suggest future studies of this sort that employ the use of more infrasound sensors and attempt to place them in other configurations. Additional infrasound sensors, particularly in February, would have provided the ability to track changes from February to August solely using the BPSC and HPSC methods. In August the sensors were aligned towards the vent, which allowed for good temporal resolution. However, Johnson et al. (2008) and Kim et al. (2012) have shown that it is useful to place sensors around the vent in order to improve the spatial resolution and stability of the inversion. Using this configuration, one can investigate the possibility of a non-monopole component in the slug bursts. If such a component is found in the slug burst events, then a more complex source model would give more accurate source estimates.

Collecting gas measurements as a means to "calibrate" the monopole source inversion is also suggested. Dalton et al. (2010) show that making concurrent gas and acoustic measurements allows for a comparison between calculated and observed total emissions values. At Pacaya the results were promising, falling within an order of magnitude of one another. Obtaining a multiparameter dataset at Tolbachik Volcano would have allowed for emissions correlation, and would ultimately have given insight into the adequacy of the monopole source inversion method. Future work along these lines is suggested to validate infrasound-based emissions calculations.

Conclusion

Chapter 1 presents research at Tolbachik Volcano that gives insight into the total volume of emissions from individual gas slug burst events. These volumes provide three possible scenarios for eruption dynamics at Tolbachik Volcano from mid-February to late August 2013: 1) the eruption stays consistent through time, 2) the eruption transitions from dominantly slug bursts in February to a mixture of roiling within the lava lake and slug bursting in August and 3) the eruption transitions from dominantly slug bursts in February to a mixture of roiling within the lava lake and slug bursting in August, but fewer explosions occurring overall. Total emissions volumes were calculated for individual slug burst events and are smaller than those calculated from infrasound measurements at Mt. Erebus Volcano, Antarctica in 2006, but larger than those calculated at Pacaya Volcano, Guatemala in 2010.

Future studies in volcano infrasound will likely investigate eruption dynamics using many different approaches. Understanding eruption dynamics allows for a better understanding of volcanic processes and is key to hazard mitigation. Infrasound studies will likely aid in a better understanding of eruption dynamics. Acoustic waveforms may hold the key to understanding eruption dynamics, and if so would allow for quick and informed decision making to mitigate hazards.

An adequate event picking method to detect volcanic eruptions is essential in these studies. In the "Additional Analysis and Future Work" section we implement the Short Term Average Long Term Average event picking method, though others methods may be useful as well. After picking events, waveform families are determined using waveform cross correlation. Families are then correlated with observed activity at the volcano in order to determine a relationship between acoustic waveforms and eruption characteristics. The next section offers additional details and suggestions, as well as suggestions for future work.

C.1 Additional Analysis and Future Work

In August 2011 a multiparameter dataset was collected at Karymsky Volcano, Kamchatka, Russia (Fig. C.1.1a) that includes infrasound data, gas and ash data, and thermal imagery from eruptive events (Lopez et al., 2013). Lopez et al. (2013) determined four distinct eruption styles at Karymsky Volcano during this time period using these data. The knowledge of four eruption styles at Karymsky Volcano presents a rare opportunity to investigate the relationship between infrasound waveforms and a wide variety of volcanic processes. A well-understood relationship between infrasound waveforms and eruption characteristics would prove particularly useful at difficult-to-monitor volcanoes. Here we present additional analysis that explores the multiparameter dataset from Karymsky Volcano in August 2011 and infrasound data collected at Sakurajima Volcano (Fig. C.1.1b) in July 2013. Infrasound data array data were collected from four sensors at Karym-

sky Volcano during August 15-21, 2011. Five infrasound sensors, placed in a network configuration around Sakurajima Volcano, collected data from July 18-26, 2013 (Fee et al., 2014). However, only three of these sensors are used due to the effects of complicated topography surrounding the vent. The three sensors we used, HAR, KUR, and SVO, showed the least complications when time-aligning using cross correlation. Karymsky infrasound array data are processed in the same way as the Sakurajima data in order to maintain consistency in our methods.

Correlations between acoustic waveforms and plume characteristics give insight into how an acoustic waveform reflects various eruption processes. Lopez et al. (2013) determined relationships between these parameters for all four types of activity at Karymsky volcano. Similar relationships are determined from this study with individual waveforms. Acoustic waveform families are correlated with the plume characteristics, including temperature, maximum and mean thermal energies, amount of ash, and emission rates of SO_2. We also attempt to characterize Sakurajima waveform families using emissions data from Karymsky waveform families. We suggest that current and future research explore whether infrasound waveform correlation is a viable tool for eruption characterization. Knowing the general shape and frequency content of an infrasound waveform from a particular eruption style would be useful for hazard mitigation at difficult-to-monitor volcanoes with strategically placed regional infrasound arrays. This would essentially allow for near real-time eruption characterization.

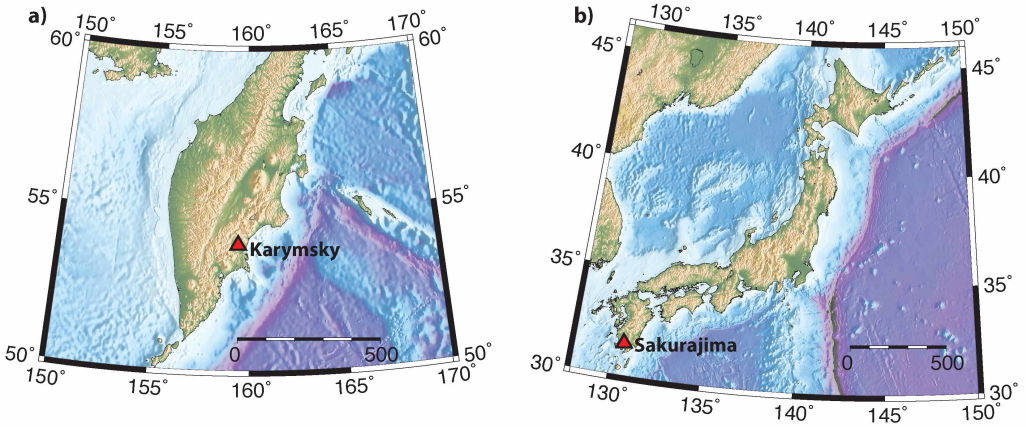

Figure C.1.1: Study area locations. a) Karymsky Volcano, Kamchatka, Russia and b) Sakurajima Volcano, Japan. In both maps the location of the active vent is given by a red triangle.

C.2 Methods

C.2.1 Event Family Classification

The variety and similarity of eruptive styles at Karymsky and Sakurajima volcanoes makes a family classification scheme desirable. Previous seismic waveform classification studies have given insight into the relationship between family occurrence and volcanic activity (Green et al., 2013; Green and Neuberg, 2006; Petersen, 2007; Stephens and Chouet, 2001). However, this has yet to be done with volcano infrasound data, possibly due to large variations in acoustic waveforms. Matoza et al. (2014) did a similar analysis at Sakurajima, Karymsky, and Tungruhua Volcanoes using infrasound characteristics to characterize explosive complexity, but do not go into great detail on how waveform shape is affected by volcanic emissions.

Following the method of Green and Neuberg (2006), tour initial step is to identify a master waveform for the first family. This is done by finding the autocorrelation and cross correlation coefficients for each event with all other events. The event with the highest mean correlation coefficient (i.e. the event that is most similar to all events) is chosen as the master waveform for Family 1 (Green and Neuberg, 2006; Stephens and Chouet, 2001). All events that show a high correlation with the master waveform are regarded as belonging to Family 1. In this study a cross correlation coefficient greater than 0.6 is enough to consider an event part of the family. The members of Family 1 are extracted from the event matrix in order to find new master waveforms for subsequent families (Green and Neuberg, 2006; Stephens and Chouet, 2001). A similar selection procedure is then used to determine additional waveform families. Figure C.2.1 shows an example of the waveform family classification process.

When first implementing this method on all of the events detected at Karymsky Volcano, distinct families did not emerge. Instead, to identify waveform families from each eruption type, we choose to focus on the events occurring during the time periods described by Lopez et al. (2013) as characteristic for a particular eruption type. During August 2011 only three types of eruptive activity occurred: discrete ash explosions, pulsatory degassing, and explosive eruptions (Lopez et al., 2013). These three time periods contain only one waveform family each. By applying the aforementioned method we find that during these three time periods only one waveform family exists for each. Once waveform families are determined for each specific time period, the master waveforms from each family are cross correlated with all Karymsky events identified between August 15-22, 2011. Events with a cross correlation value greater than 0.8 (or 0.9 for the explosive eruptions) are grouped into the corresponding master waveform's family of ash explosions, pulsatory degassing, or explosive eruptions.

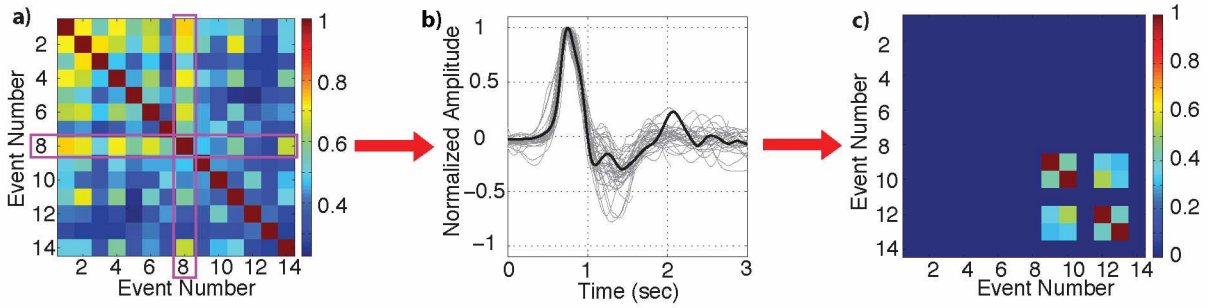

Figure C.2.1: Cross correlation using a master waveform. a) All events are cross correlated with one another (including themselves). The event with the highest mean cross correlation value is chosen as the first master waveform (shown by the magenta boxes). b) Events that display a cross correlation value greater than 0.6 are chosen as members of the first family. The black line shows the master waveform and the gray lines show the members of the family. Waveform amplitudes are normalized. c) Members of the first family are removed from the cross correlation matrix. The process begins again with a new master waveform. In this case, there are no similar waveforms to make up a second family.

C.2.2 Event Identification

Data are first band-pass filtered using limits selected to avoid waveform contamination by the filtering process. When filter limits are close to dominant signal frequencies, artifacts from filtering can be seen in waveform onsets (Scherbaum and Bouin, 1997). These filtering artifacts are so highly correlated that they alter the construction of waveform families. Therefore, filtering limits are set as far as possible from dominant signal frequencies while still avoiding noise contamination. Filtering limits for explosive eruptions and ash-rich explosions are 0.3-5 Hz and 0.5-5 Hz for pulsatory degassing events. These limits are listed in Table C.2.1.

The nature of large amplitude event onsets at Karymsky and Sakurajima Volcanoes allows for a relatively simple detection method. The Short Term Average Long Term Average (STA/LTA) ratio is used to identify events at Karymsky and Sakurajima volcanoes. The STA/LTA ratio can be defined by the following equations:

$$\mathrm{STA} = \frac{x_i^2 - x_{i-N_{\mathrm{sta}}}^2}{N_{\mathrm{sta}}} + \mathrm{STA}_{i-1} \tag{C.2.1}$$

$$\mathrm{LTA} = \frac{x_{i-N_{\mathrm{sta}}-1}^2 - x_{i-N_{\mathrm{sta}}-N_{\mathrm{lta}}-1}^2}{N_{\mathrm{lta}}} + \mathrm{LTA}_{i-1} \tag{C.2.2}$$

where x corresponds to the time series dataset, i is the time index $(1, 2, 3, \ldots, n = \text{length of dataset})$, and N_{sta} and N_{lta} correspond to the STA and LTA window lengths respectively (Withers

et al., 1998). Typically values for STA window lengths correspond to the average duration of an event while values for LTA window lengths correspond to the average duration of noise between events. However, for both the Karymsky and Sakurajima data, $N_{\text{sta}} = 1$ s, $N_{\text{lta}} = 120$ s. Events at both volcanoes last longer than 1 s, but we choose to focus on the first second of each eruption as this contains the least attenuated part of the waveform. The number of events at Karymsky and Sakurajima are too numerous to be picked by hand, but are easily identifiable by eye. Therefore, an STA/LTA threshold is determined using the easily identifiable events as a guide. A threshold of 1 is set to identify events at Karymsky Volcano. At Sakurajima Volcano the threshold is higher, chosen as 30. Event length is determined from a user-defined pre event time (PEM) and post event time (PET). Therefore, the onset time of the event is equal to the time where the ratio exceeds the threshold minus the PEM. For events at both volcanoes, PEM and PET values are 10 s and 16 s, making events 26 s in duration. The PEM and PET parameter values were chosen using a few randomly selected events in the data. Automatic picks were manually inspected to determine adequate values.

After identification using the STA/LTA, the signal-to-noise ratio (SNR) of each possible event is analyzed. Because the STA/LTA method uses only one sensor out of the group of infrasound sensors, this is done to mitigate the possibility of a false trigger. The Fisher Statistic (F-statistic) gives a measure of the signal-to-noise ratio (SNR) and is computed for each event. The F-statistic is defined as:

$$F = \frac{N-1}{N} \frac{\Sigma_{t=1}^{M} u(t)^2}{\frac{1}{N}\Sigma_{t=1}^{M}\Sigma_{i=1}^{N} u_i(t)^2 - \Sigma_{t=1}^{M} u(t)^2} \tag{C.2.3}$$

where $u_i(t)$ is the time-shifted output of sensor i at time t, $u(t)$ is the mean of the outputs from N sensors at time t, and M corresponds to the number of points in the window (Blandford, 1974). The F-statistic is related to the SNR by $\text{SNR} = \frac{1}{N}(F-1)$. A F-statistic threshold of 5 (i.e. $\text{SNR} > 1$) is used in order to identify events from Karymsky Volcano. An F-statistic threshold of 4 ($\text{SNR} > 1$) is used to detect events from Sakurajima Volcano. After events are identified, they are stored in a matrix for subsequent analysis. Filtering limits, STA/LTA inputs, and F-statistic thresholds for each volcano and/or event type are summarized in Table C.2.1.

C.3 Results

Three waveform families are identified at Karymsky Volcano and one family is identified at Sakurajima Volcano using the previously described methods. The waveform families at Karymsky Volcano correspond to those eruption types identified by Lopez et al. (2013) and were expected to arise out of the usage of the previous methods and time periods. The waveform family for ash explosions displays a compression followed by a small rarefaction. Distinct "double troughs"

Table C.2.1: Analysis inputs for event identification at Karymsky and Sakurajima Volcanoes.

Inputs	Karymsky Volcano	Sakurajima Volcano
Filter Limits	Explosive Eruptions: 0.3 - 5 Hz Ash-rich Explosions: 0.3 - 5 Hz Pulsatory Degassing: 0.5 - 5 Hz	0.1 - 10 Hz
STA Window	1 second	1 second
LTA Window	120 seconds	120 seconds
Pre-Event Time (PEM)	10 seconds	10 seconds
Post-Event Time (PET)	16 seconds	16 seconds
Trigger	1	20
F-statistic Threshold	5	2

are present in the rarefaction and the dominant frequency is 0.2-10 Hz (Fig. C.3.1a). Pulsatory degassing waveforms are characterized by a sharp compression followed by a smaller rarefaction. The dominant frequency for these waveforms is 1-10 Hz (Fig. C.3.1b). The waveform family from the explosive eruptions shows a sharp compression and an equal rarefaction (Fig. C.3.1c). These events were large in amplitude and two consequently clipped the sensors where amplitudes were greater than 125 Pa. These clipped events were removed from the waveform family matrix prior to plotting. Only one waveform family is identified at Sakurajima Volcano. This family shows a sharp compression followed by a slightly smaller rarefaction. Waveforms in this family show a lower dominant frequency of 0.3-0.5 Hz (Fig. C.3.1d). The waveform family from Sakurajima Volcano does not correlate well with any of the three families from Karymsky Volcano.

Infrasound and emissions correlation at Karymsky Volcano allows for conclusions to be drawn about the possibility of eruption characteristics correlating with the shape of an infrasound waveform. Master waveforms from each family are correlated with the emissions data from Lopez et al. (2013) for the corresponding eruption type. Ash explosions at Karymsky are characterized as discrete ash-rich explosions occurring from the vent. Ash explosions at Karymsky are described as discrete ash-rich explosions occurring from the vent. Plume heights reach 500-1500 m with maximum temperatures of 230 $\pm$ 60 ° C. The mean SO_2 emission rate for ash explosion events is >0.7 $\pm$ 0.4 kg/s. Pulsatory degassing events show little to no ash and occur as individual pulses. Plume heights reach 100-200 m altitude with a maximum plume temperature of 160 $\pm$ 40 °C. Mean SO_2 emission rate for pulsatory degassing events is 1.4 $\pm$ 0.8 kg/s. Explosive eruptions are ash-rich and

contain ballistics. Often there is a period of quiescence prior to the explosions. Plume heights reach >2000 m with maximum temperatures >350 °C. Mean SO_2 emission rate is 0.3 ± 0.3 kg/s (Lopez et al., 2013). Table C.3.1 provides a comprehensive list of emissions data and acoustic waveforms for each eruption type at Karymsky Volcano.

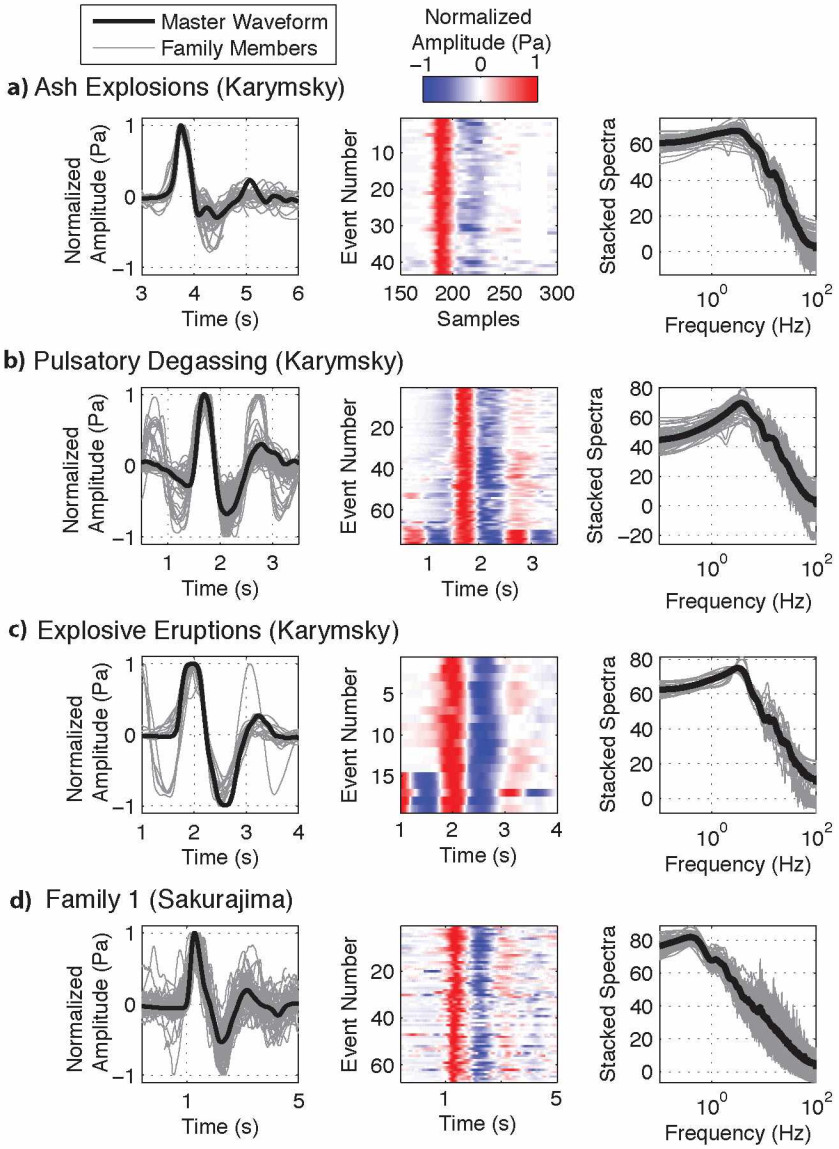

Figure C.3.1: Waveform families at Karymsky and Sakurajima Volcanoes. Waveform family members (gray) with master waveforms (black), plots showing amplitudes of waveforms for each family, and stacked spectra from each family for a) ash explosions, b) pulsatory degassing, and c) explosive eruptions at Karymsky Volcano, and d) Family 1 at Sakurajima Volcano. All waveform amplitudes are normalized.

Table C.3.1: Emissions correlation with Karymsky waveforms.

Eruption Type	Ash Explosions	Pulsatory Degassing	Explosive Eruptions
Gas/Ash Content	Ash-rich	Little to no ash	Ash-rich, ballistics
General Characteristics	Discrete explosions from the vent	Individual pulses	Quiescence followed by large explosion
Altitude Above Vent	500 m - 1500 m	100 m - 200 m	$>$ 2000 m
Maximum Plume Temperature	230° $\pm$ 60° C	160° $\pm$ 40 C	$>$ 350° C
Mean SO_2 Emission Rate	$>$ 0.7 $\pm$ 0.4 kg/s	1.4 $\pm$ 0.8 kg/s	0.3 $\pm$ 0.3 kg/s
Acoustic Waveform	See Fig. 3.5a	See Fig. 3.5b	See Fig. 3.5c

C.4 Discussion

The presence of three families for three distinct eruption types at Karymsky Volcano gives promising results for the future of eruption characterization using acoustic waveforms. Three distinct waveform families correspond to the three different event types observed at the volcano during this time period: ash explosions, pulsatory degassing, and explosive eruptions. Results suggest that individual eruption characteristics related to the three different event types affect the shape of an acoustic waveform. Only one waveform family is found at Sakurajima Volcano. The master waveform from this family does not correlate well with any of the families found at Karymsky Volcano. This is surprising as the eruption style of Sakurajima Volcano is similar to that of Karymsky Volcano. Activity at both volcanoes ranges from short-duration, ash-rich, explosions to longer-duration ash-rich explosions (Lopez et al., 2013). Not much can be determined from the Sakurajima family alone until future work allows for better waveform comparison.

While only one family was found from eruptive events at Sakurajima Volcano, visual observations (Matoza et al., 2014) suggest there are likely more event types that occurred but were not identified, such as volcanic jetting. However, volcanic jetting may not have a characteristic waveform associated with it. Even if volcanic jetting did have a characteristic waveform shape, the STA/LTA picking method is not adequate for picking events such as this because it is designed to identify impulsive onsets (Matoza et al., 2014). Therefore, only large explosive events are picked using the current inputs and method. Different STA/LTA inputs and/or implementing a

different event picking method may provide families for other activity types at Sakurajima Volcano.

While we cannot yet draw solid connections between waveform shape and eruption characteristics, these results give us a glimpse of future possibilities. For example, the distinct "double trough" shape of the ash explosions family at Karymsky Volcano may be correlated with activity that occurs as discrete ash-rich explosions occurring from the vent. The occurrence of this family might indicate that the plume rises 500-1500 m above the vent, has a maximum temperature of 230 $\pm$ 60 °C, and a mean SO_2 emission rate of 0.7 $\pm$ 0.4 kg/s. The presence of the pulsatory degassing waveform may indicate that individual pulses are occurring with little to no ash. This might indicate that the plume is 100-200 m above the vent, have a maximum temperature of 160 $\pm$ 40 °C, and a mean SO_2 emission rate of 1.4 $\pm$ 0.8 kg/s. The presence of the third waveform family, the explosive eruptions, may indicate a large ash-rich explosion with ballistics. This may suggest that the plume is >2000 m above the vent, has a maximum temperature >350 °C, and a mean SO_2 emission rate of 0.3 $\pm$ 0.3 kg/s. We attempted to correlate these eruption characteristics with the waveform family from Sakurajima. This family, however, did not correlate with any of the three families from Karymsky because it has a lower dominant frequency. Therefore, results from this study do not yet allow for the knowledge of whether the master waveforms from the three families at Karymsky Volcano apply to similar eruption styles at other volcanoes. However, more studies such as this one must be completed at other volcanoes before any solid relationships between waveform shape and eruption characteristics can be drawn.

Results from this study do not yet allow for the knowledge of whether the master waveforms from the three families at Karymsky Volcano apply to similar eruption styles at other volcanoes. The three families from Karymsky are not well correlated with the waveform family from Sakurajima Volcano because of its lower dominant frequency. Knowing the general shape and frequency content of an infrasound waveform from a particular eruption style would be useful for hazard mitigation at difficult-to-monitor volcanoes with strategically placed regional infrasound arrays. This would essentially allow for near real-time eruption characterization. However, more studies such as this one must be completed at other volcanoes before any relationships between waveform shape and eruption characteristics can be drawn.

C.5 Suggestions for Future Work

Preliminary results suggest that acoustic waveforms show promise as a tool for eruption characterization at Karymsky Volcano. Three independent waveform families are correlated with three different eruption styles, showing that the shape of acoustic waveforms is related to the general eruption style. Waveform family characterization and emissions correlation should be further investigated at these and other volcanoes. This would allow for determination of the usefulness of acoustic waveforms in characterizing eruption dynamics.

It is essential that future studies implement multiparameter datasets such as the one collected at Karymsky Volcano in August 2011. This will allow for investigating the effect of eruption characteristics on acoustic waveforms. Studies like this must be done at a variety of volcanoes and on a variety of eruption styles. This will facilitate the use of acoustic waveforms as tools for eruption characterization.

Determining a relationship between acoustic waveforms and eruption characteristics would be particularly useful at difficult-to-monitor volcanoes. Knowing the propagation paths of infrasound in the atmosphere allows for regional arrays to be placed in areas that allow for the detection of infrasound from specific difficult-to-monitor volcanoes. Therefore, a regional array can be placed in a pre-determined location that allows for eruption detection for a particular volcano. If a relationship between eruption characteristics and waveform shape were known, the infrasound signal could be analyzed almost immediately to estimate plume height, temperature, and ash content as well as mean SO_2 emission rate and general eruption type. Essentially this would allow for near real-time eruption characterization and may hold the key to remote hazard characterization and/or mitigation using infrasound.

It is essential that future studies implement multiparameter datasets such as the one collected at Karymsky Volcano in August 2011. This will allow for investigations on the effects eruption characteristics have on acoustic waveforms. Studies like this must be done at a variety of volcanoes with a variety of eruption styles in order to allow for the opportunity of using acoustic waveforms as tools for eruption characterization. Determining a relationship between acoustic waveforms and eruption characteristics would be useful at difficult-to-monitor volcanoes with strategically placed regional arrays that allow for adequate atmospheric propagation of infrasound. This would allow for near real-time eruption characterization and may hold the key to remote hazard characterization and/or mitigation.

References

Aiuppa, A., Federico, C., Paonita, A., Pecoraino, G., and Valenza, M. (2002). S, Cl and F degassing as an indicator of volcanic dynamics: The 2001 eruption of Mount Etna. *Geophys. Res. Lett.*, 29(11).

Aki, K., Fehler, M., and Das, S. (1977). Source mechanism of volcanic tremor: fluid-driven crack models and their application to the 1963 Kilauea eruption. *J. Volcanol. Geotherm. Res.*, 2(3):259–287.

Anstey, N. (1964). Correlation techniques - a review. *Geophys. Prospect.*, 12(4):55–82.

Blandford, R. (1974). An automatic event detector at the Tonto Forest seismic observatory. *Geophys.*, 39:633–643.

Braitseva, O. A., Ponomareva, V. V., Sulerzhitsky, L. D., Melekestsev, I. V., and Bailey, J. (1997). Holocene key-marker tephra layers in Kamchatka, Russia. *Quat. Res.*, 47(2):125–139.

Brandeis, G., Ooi, W., Hossain, M., Morris, J., and Lipsitz, L. (1994). A longitudinal-study of risk-factors associated with the formation of pressure ulcers in nursing-homes. *J. Am. Geriatr. Soc.*, 42(4):388–393.

Buckingham, M. J. and Garces, M. A. (1996). Canonical model of volcano acoustics. *J. Geophys. Res.-Solid Earth*, 101(B4):8129–8151.

Casadevall, T. J. (1994). The 1989-1990 eruption of Redoubt Volcano, Alaska - impacts on aircraft operations. *J. Volcanol. Geotherm. Res.*, 62(1-4):301–316.

Casadevall, T. J., Delos Reyes, P. J., and Schneider, D. J. (1996). *The 1991 Pinatubo eruptions and their effects on aircraft operations.*, pages 625–636.

Casadevall, T. J., Doukas, M. P., Neal, C. A., McGimsey, R. G., and Gardner, C. A. (1994). Emission rates of sulfur dioxide and carbon dioxide from Redoubt Volcano, Alaska during the 1989-1990 eruptions. *J. Volcanol. Geotherm. Res.*, 62:519–530.

Chouet, B. (1985). Excitation of a buried magmatic pipe - a seismic source model for volcanic tremor. *J. Geophys. Res.-Solid Earth and Planets*, 90(2):1881–1893.

Cronin, S. J., Manoharan, V., Hedley, M. J., and Loganathan, P. (2000). Fluoride: A review of its fate, bioavailability, and risks of fluorosis in grazed-pasture systems in New Zealand. *New Zealand J. Agr. Res.*, 43(3):295–321.

Dalton, M. P., Waite, G. P., Watson, I. M., and Nadeau, P. A. (2010). Multiparameter quantification of gas release during weak Strombolian eruptions at Pacaya Volcano, Guatemala. *Geophys. Res. Lett.*, 37.

Donn, W. and Rind, D. (1972). Microbaroms and the temperature and wind of the upper atmosphere. *J. Atmos. Sci.*, 29:156–172.

Fedotov, S., Utkin, I., and Utkina, L. (2011). The peripheral magma chamber of Ploskii Tolbachik, a Kamchatka Basaltic Volcano: Activity, location and depth, dimensions, and their changes based on magma discharge observations. *J. Volcanol. Seismol.*, 5(6):369–385.

Fee, D., Garces, M., and Steffke, A. (2010). Infrasound from Tungurahua Volcano 2006-2008: Strombolian to Plinian eruptive activity. *J. Volcanol. Geotherm. Res.*, 193(1-2):67–81.

Fee, D. and Matoza, R. S. (2013). An overview of volcano infrasound: From hawaiian to plinian, local to global. *J. Volcanol. Geotherm. Res.*, 249:123–139.

Fee, D., Yokoo, A., and Johnson, J. (2014). Introduction to an open community infrasound dataset from the actively erupting Sakurajima Volcano, Japan. *Seism. Res. Lett.*, 85(6):1–11.

Firstov, P. and Kravchenko, N. (1996). Estimation of the amount of explosive gas released in volcanic eruptions using air waves. *Volcanol. Seismol.*, 17:547–560.

Firstov, P. P. (1996). Wave disturbances in the atmosphere as a source of information on the dynamics of volcanic eruptions. *Eos*, 318(3):813.

Fischer, T. P. (2008). Fluxes of volatiles (H_2O, CO_2, N^{-2}, Cl, F) from arc volcanoes. *Geochem. J.*, 42(1):21–38.

Fraunfelder, F. T., Kalina, R. E., Buist, A. S., Bernstein, R. S., and Johnson, D. S. (1983). Ocular effects following the volcanic-eruptions of Mount St-Helens. *Arch. Ophthalmol.*, 101(3):376–378.

Garces, M., Iguchi, M., Ishihara, K., Morrissey, M., Sudo, Y., and Tsutsui, T. (1999). Infrasonic precursors to a Vulcanian eruption at Sakurajima Volcano, Japan. *Geophys. Res. Lett.*, 26(16):2537–2540.

Gordeev, E., Murav'ev, Y., Samoilenko, S., Volynets, A., Mel'nikov, D., and Dvigalo, V. (2013). First results from the 2012-2013 Tolbachik fissure eruption. *Bull. Volcano. Soc. Japan*, 58(2):1–8.

Green, D. N., Evers, L. G., Fee, D., Matoza, R. S., Snellen, M., Smets, P., and Simons, D. (2013). Hydroacoustic, infrasonic and seismic monitoring of the submarine eruptive activity and subaerial plume generation at South Sarigan, May 2010. *J. Volcanol. Geotherm. Res.*, 257:31–43.

Green, D. N. and Neuberg, J. (2005). Seismic and infrasonic signals associated with an unusual collapse event at the Soufriere Hills Volcano, Montserrat. *Geophys. Res. Lett.*, 32(7).

Green, D. N. and Neuberg, J. (2006). Waveform classification of volcanic low-frequency earthquake swarms and its implication at Soufriere Hills Volcano, Montserrat. *J. Volcanol. Geotherm. Res.*, 153(1-2):51–63.

Gresta, S., Ripepe, M., Marchetti, E., D'Amico, S., Coltelli, M., Harris, A. L. J., and Privitera, E. (2004). Seismoacoustic measurements during the July-August 2001 eruption of Mt. Etna Volcano, Italy. *J. Volcanol. Geotherm. Res.*, 137(1-3):219–230.

Gudmundsson, M., Pedersen, R., Vogfjörd, K., Thorbjarnardóttir, B., Jakobsdóttir, S., and Roberts, M. (2010). Eruptions of eyjafjallajökull volcano, iceland. *Eos*, 9(21):190–191.

Hagerty, M., Protti, M., Schwartz, S., and Garces, M. (2000). Analysis of seismic and acoustic observations at Arsenal Volcano, Costa Rica. *J. Volcanol. Geotherm. Res.*, 121(1-2):15–63.

Horwell, C. J. and Baxter, P. J. (2006). The respiratory health hazards of volcanic ash: a review for volcanic risk mitigation. *Bull. Volcanol.*, 69(1):1–24.

Inbar, M., Gilichinsky, M., Melekestsev, I., Melnikov, D., and Zaretskaya, N. (2011). Morphometric and morphological development of Holocene cinder cones: A field and remote sensing study in the Tolbachik volcanic field, Kamchatka. *J. Volcanol. Geotherm. Res.*, 201(1-4):301–311.

Johnson, J., Aster, R., Jones, K. R., Kyle, P., and McIntosh, B. (2008). Acoustic source characterization of impulsive Strombolian eruptions from the Mount Erebus lava lake. *J. Volcanol. Geotherm. Res.*, 177:673–686.

Johnson, J. B., Aster, R. C., and Kyle, P. R. (2004). Volcanic eruptions observed with infrasound. *Geophys. Res. Lett.*, 31(14).

Johnson, J. B., Aster, R. C., Ruiz, M. C., Malone, S. D., McChesney, P. J., Lees, J. M., and Kyle, P. R. (2003). Interpretation and utility of infrasonic records from erupting volcanoes. *J. Volcanol. Geotherm. Res.*, 121(1-2):15–63.

Johnson, J. B. and Ripepe, M. (2011). Volcano infrasound: A review. *J. Volcanol. Geotherm. Res.*, 206(3-4):61–69.

Kim, K., Lees, J. M., and Ruiz, M. (2012). Acoustic multipole source model for volcanic explosions and inversion for source parameters. *Geochem. J. Int.*, 191(3):1192–1204.

Lambert, G., Lecloarec, M. F., Ardouin, B., and Leroulley, J. C. (1985). Volcanic emission of radionuclides and magma dynamics. *Earth and Planetary Sci. Lett.*, 76(1-2):185–192.

Lighthill, J. (1978). *Waves in Fluids*. Cambridge University Press.

Lopez, T., Fee, D., Prata, F., and Dehn, J. (2013). Characterization and interpretation of volcanic activity at Karymsky Volcano, Kamchatka, Russia, using observations of infrasound, volcanic emissions, and thermal imagery. *Geochem. Geophys. Geosystems*, 14(12):5106–5127.

Matoza, R., Fee, D., and Lopez, T. (2014). Acoustic characterization of explosion complexity at Sakurajima, Karymsky, and Tungurahua Volcanoes. *Seism. Res. Lett.*, 85(6).

Moran, S. C., Matoza, R. S., Garces, M. A., Hedlin, M. A. H., Bowers, D., Scott, W. E., Sherrod, D. R., and Vallance, J. W. (2008). Seismic and acoustic recordings of an unusually large rockfall at Mount St. Helens, Washington. *Geophys. Res. Lett.*, 35(19).

Olson, J. (2004). The application of the Pure-State Filter to infrasound array data. *Inframatics Newsletter*, 7:15–21.

Petersen, T. (2007). Swarms of repeating long-period earthquakes at Shishaldin Volcano, Alaska, 2001-2004. *J. Volcanol. Geotherm. Res.*, 166(3-4):177–192.

Petersen, T. and McNutt, S. R. (2007). Seismo-acoustic signals associated with degassing explosions recorded at Shishaldin Volcano, Alaska, 2003-2004. *Bull. Volcanol.*, 69(5):527–536.

Ruiz, M., Lees, J. M., and Johnson, J. B. (2006). Source constraints of Tungurahua Volcano explosion events. *Bull. Volcanol.*, 68(5):480–490.

Shore, J. H., Tatum, E. L., and Vollmer, W. M. (1986). Evaluation of mental effects of disaster, Mount St-Helens eruption. *Amer. J. Public Health*, 76:76–83.

Soden, B. J., Wetherald, R. T., Stenchikov, G. L., and Robock, A. (2002). Global cooling after the eruption of Mount Pinatubo: A test of climate feedback by water vapor. *Sci.*, 296(5568):727–730.

Steffke, A. M., Fee, D., Garces, M., and Harris, A. (2010). Eruption chronologies, plume heights and eruption styles at Tungurahua Volcano: Integrating remote sensing techniques and infrasound. *J. Volcanol. Geotherm. Res.*, 193(3-4):143–160.

Stephens, C. D. and Chouet, B. A. (2001). Evolution of the December 14, 1989 precursory long-period event swarm at Redoubt Volcano, Alaska. *J. Volcanol. Geotherm. Res.*, 109(1-3):133–148.

Szuberla, C. A. L. and Olson, J. V. (2004). Uncertainties associated with parameter estimation in atmospheric infrasound arrays. *J. Acoustic. Soc. Am.*, 115(1):253–258.

Ulivieri, G., Ripepe, M., and Marchetti, E. (2013). Infrasound reveals transition to oscillatory discharge regime during lava fountaining: Implication for early warning. *Geophys. Res. Lett.*, 40(12):3008–3013.

Vergniolle, S., Boichu, M., and Caplan-Auerbach, J. (2004). Acoustic measurements of the 1999 basaltic eruption of Shishaldin Volcano, Alaska - 1. origin of strombolian activity. *J. Volcanol. Geotherm. Res.*, 137(1-3):109–134.

Werner, C., Kelly, P. J., Doukas, M., Lopez, T., Pfeffer, M., McGimsey, R., and Neal, C. (2013). Degassing of CO_2, SO_2, and H_2S associated with the 2009 eruption of Redoubt Volcano, Alaska. *J. Volcanol. Geotherm. Res.*, 259:270–284.

Withers, M., Aster, R., Young, C., Beiriger, J., Harris, M., Moore, S., and Trujillo, J. (1998). A comparison of select trigger algorithms for automated global seismic phase and event detection. *Bull. Seismol. Soc. Am.*, 88(1):95–106.

Yamasato, H. (1998). Nature of infrasonic pulse accompanying low frequency earthquake at Unzen Volcano, Japan. *Bull. Volcanol. Soc. Japan*, 43:1–13.

Zelenski, M., Malik, N., and Taran, Y. (2014). Emissions of trace elements during the 2012-2013 effusive eruption of Tolbachik Volcano, Kamchatka: enrichment factors, partition coefficients and aerosol contribution. *J. Volcanol. Geotherm. Res.*, 285:136–149.